

## Supporting Information

### **Fabrication of thiosemicarbazone based Pd(II) complexes: structural elucidations, catalytic activity towards Suzuki-Miyaura coupling reaction and antitumor activity against TNBC cells**

*Biswajit Bera,<sup>†</sup> Pulak Jana,<sup>§□</sup> Subrata Mandal,<sup>†</sup> Sudip Kundu,<sup>‡</sup> Akash Das,<sup>†</sup> Krishnananda Chattopadhyay,<sup>§</sup> Tapan Kumar Mondal<sup>†\*</sup>*

<sup>†</sup> Department of Chemistry, Jadavpur University, Kolkata 700032, India.

<sup>§</sup> Structural Biology & Bio-Informatics Division, CSIR-Indian Institute of Chemical Biology, 4, Raja S. C. Mallick Road, Kolkata 700032, India.

<sup>□</sup> Academy of Scientific and Innovative Research (AcSIR), Ghaziabad, Uttar Pradesh 201002, India.

<sup>‡</sup> School of Materials Science and Nanotechnology, Jadavpur University, Kolkata 700032, India.

### CONTENTS

#### Experimental Section

Scheme S1: Synthesis routes of the ligands **H<sub>2</sub>L<sup>1</sup>**, **H<sub>2</sub>L<sup>2</sup>** and **HL<sup>3</sup>**

Figure S1: ORTEP view of ligand **HL<sup>3</sup>** with 50% ellipsoidal probability

Figure S2: 2D supramolecular arrangement of ligand **HL<sup>3</sup>**

Figure S3: 3D architecture of **C1** shows hydrogen bonds and  $\pi\cdots\pi$  interactions

Figure S4: 3D supramolecular aggregate of **C2** along 'b' axis

Figure S5: <sup>1</sup>H-NMR spectrum of **H<sub>2</sub>L<sup>1</sup>** in DMSO-d<sub>6</sub>

Figure S6: <sup>13</sup>C-NMR spectrum of **H<sub>2</sub>L<sup>1</sup>** in DMSO-d<sub>6</sub>

Figure S7: <sup>1</sup>H-NMR spectrum of **H<sub>2</sub>L<sup>2</sup>** in DMSO-d<sub>6</sub>

Figure S8: <sup>13</sup>C-NMR spectrum of **H<sub>2</sub>L<sup>2</sup>** in DMSO-d<sub>6</sub>

Figure S9: <sup>1</sup>H-NMR spectrum of **HL<sup>3</sup>** in DMSO-d<sub>6</sub>

Figure S10: <sup>13</sup>C-NMR spectrum of **HL<sup>3</sup>** in DMSO-d<sub>6</sub>

Figure S11: <sup>1</sup>H-NMR spectrum of **C1** in DMSO-d<sub>6</sub>

Figure S12: <sup>1</sup>H-NMR spectrum of **C2** in DMSO-d<sub>6</sub>

Figure S13: <sup>1</sup>H-NMR spectrum of **C3** in DMSO-d<sub>6</sub>

Figure S14: HRMS of **H<sub>2</sub>L<sup>1</sup>** in acetonitrile

Figure S15: HRMS of **H<sub>2</sub>L<sup>2</sup>** in acetonitrile

Figure S16: HRMS of **HL<sup>3</sup>** in acetonitrile

Figure S17: HRMS of **C1** in acetonitrile

Figure S18: HRMS of **C2** in acetonitrile

Figure S19: HRMS of **C3** in acetonitrile

Figure S20: IR spectra of **H<sub>2</sub>L<sup>1</sup>**, **H<sub>2</sub>L<sup>2</sup>** and **HL<sup>3</sup>**

Figure S21: IR spectra of **C1**, **C2** and **C3**

Figure S22: UV-Vis spectra of (a) **H<sub>2</sub>L<sup>1</sup>** and **C1**, (b) **H<sub>2</sub>L<sup>2</sup>** and **C2** and (c) **HL<sup>3</sup>** and **C3** in acetonitrile

Figure S23: Time-dependent UV-Vis spectra of complexes (**C1 – C3**) in DMSO at room temperature

Figure S24: Time-dependent UV-Vis spectra of complexes (**C1 – C3**) in Tris-HCl/NaCl buffer (pH = 7.4) at room temperature

Figure S25: UV-Vis titration plot of **C1** with the gradual addition of CT-DNA

Figure S26: UV-Vis titration plot of **C2** with the gradual addition of CT-DNA

Figure S27: Fluorescence titration of EB-CT DNA with the increasing amount of **C1**

Figure S28: Fluorescence titration of EB-CT DNA with the increasing amount of **C2**

Figure S29: Effect of increasing concentrations of EB and complexes (**C1–C3**) on the relative viscosity of CT-DNA

Figure S30: Fluorescence quenching titration of BSA with incremental addition of **C1**

Figure S31: Fluorescence quenching titration of BSA with incremental addition of **C2**

Figure S32: CD spectra of free BSA and BSA in presence of equimolar concentration of complexes **C1–C3**

Figure S33: FRET between BSA and complexes (a) **C1**, (b) **C2** and (c) **C3**

Figure S34: Viability of HepG2 cells were assessed by treating different doses of complexes **C1–C3**

Table S1: Crystallographic data and refinement parameters of **HL<sup>3</sup>**, **C1**, **C2** and **C3**

Table S2: Selected X-ray and calculated bond distances (Å) and angles (°) of **C1** and **C2**

Table S3: Selected X-ray and calculated bond distances and angles of **HL<sup>3</sup>**

Table S4: Energy and % of composition of some selected molecular orbitals of [Pd(**HL<sup>1</sup>**)Cl] (**C1**)

Table S5: Energy and % of composition of some selected molecular orbitals of [Pd(L<sup>2</sup>)PPh<sub>3</sub>]  
(C2)

Table S6: Energy and composition of some selected molecular orbitals of [Pd(L<sup>3</sup>)(PPh<sub>3</sub>)]Cl  
(C3)

Table S7: Vertical electronic transition calculated by TDDFT/CPCM method of C1, C2, C3 and  
HL<sup>3</sup>

Figure S35: Contour plots of some selected molecular orbital of C1

Figure S36: Contour plots of some selected molecular orbital of C2

Figure S37: Contour plots of some selected molecular orbital of C3

Figure S38: Contour plots of some selected molecular orbital of HL<sup>3</sup>

Table S8: Optimization of reaction conditions using catalyst C1 for the model reaction

Table S9: Optimization of reaction conditions using catalyst C3 for the model reaction

Figure S39: <sup>1</sup>H NMR of biphenyl

Figure S40: <sup>1</sup>H NMR of 4-methyl-1,1'-biphenyl

Figure S41: <sup>1</sup>H NMR of 4-methoxy-1,1'-biphenyl

Figure S42: <sup>1</sup>H NMR of 4-nitro-1,1'-biphenyl

Figure S43: <sup>1</sup>H NMR of [1,1'-biphenyl]-4-carbaldehyde

Table S10: Comparison of catalytic efficiency and reaction conditions of Suzuki-Miyaura  
cross-coupling reactions by palladium complexes with O N S donor ligands

## Experimental section

### Materials and methods

All reagents and solvents used in this synthesis were purchased from Aldrich. All other organic chemicals and inorganic salts were available from commercial sources and used without further purification.  $^1\text{H}$ , and  $^{13}\text{C}$  NMR spectra were recorded on Bruker 300 MHz and 400 MHz instruments (mentioned in each spectrum) in DMSO- $d_6$  solvent. HRMS mass spectra were recorded on Waters quadruple time-of-flight mass spectrometer (Xevo G2 Q-TOF). Electronic spectra were taken on a Shimadzu UV-1900i spectrophotometer. IR spectra were recorded on PerkinElmer Spectrum Two FT-IR Spectrometer.

### Synthesis of (E)-2-((8-hydroxyquinolin-2-yl)methylene)-N-phenylhydrazine-1-carbothioamide ( $\text{H}_2\text{L}^1$ )

A methanolic solution of 4-phenylthiosemicarbazide (0.1 g, 0.6 mmol) was added to a solution of 8-hydroxyquinoline-2-carbaldehyde (0.103 g, 0.6 mmol) in methanol and the resulting mixture was refluxed for 2 h. After the completion of the reaction a light brown colour precipitate was appeared which was filtered and washed with methanol. The yield was 0.14 g (75%).

Anal. Calc. for  $\text{C}_{17}\text{H}_{14}\text{N}_4\text{OS}$ : C, 63.34; H, 4.38; N, 17.38. Found: C, 63.39; H, 4.41; N, 17.45.  $^1\text{H}$  NMR (400 MHz, DMSO- $d_6$ ):  $\delta$  7.12 (d,  $J$  = 7.24 Hz, 1H), 7.25 (t,  $J$  = 7.28 Hz, 1H), 7.39-7.45 (m, 3H), 7.57 (d,  $J$  = 7.88 Hz, 2H), 8.31 (d,  $J$  = 8.7 Hz, 2H), 8.39 (s, 1H), 8.6 (d,  $J$  = 8.68 Hz, 1H), 9.9 (s, 1H), 10.38 (s, 1H), 12.26 (s, 1H).  $^{13}\text{C}$  NMR (75 MHz, DMSO- $d_6$ ) in ppm:  $\delta$  112.6, 118.26, 119.22, 126.15, 126.83, 128.63, 129.35, 136.58, 138.7, 139.46, 143.45, 152.18, 153.93, 177.05. IR ( $\text{cm}^{-1}$ ) in KBr: 3624  $\nu$ (O-H); 3398, 3256  $\nu$ (N-H); 3122, 2971  $\nu$ (C-H); 1592  $\nu$ (C=N); 1200  $\nu$ (C=S). HRMS: Calculated for  $\text{C}_{17}\text{H}_{15}\text{N}_4\text{OS}$  [ $\text{M} + \text{H}$ ] $^+$  ( $m/z$ ): 323.0967; found: 323.1104. UV-Vis (in  $\text{CH}_3\text{CN}$ ),  $\lambda_{\text{max}}$  ( $\epsilon$ ,  $\text{M}^{-1}\text{cm}^{-1}$ ): 346 (29944), 310 (26196), 257 (15473).

### Synthesis of (E)-2-(1-(4-hydroxy-2-oxo-2H-chromen-3-yl)ethylidene)-N-phenylhydrazine-1-carbothioamide ( $\text{H}_2\text{L}^2$ )

0.1 g (0.5 mmol) of 3-acetyl-4-hydroxycoumarin was dissolved in 8 mL methanol, to it 0.083 g (0.5 mmol) 4-phenylthiosemicarbazide was added and the mixture was refluxed for 2 h. A light-yellow precipitate was appeared which is filtered and washed with methanol. The yield was 0.124 g (72%).

Anal. Calc. for  $\text{C}_{18}\text{H}_{15}\text{N}_3\text{O}_3\text{S}$ : C, 61.18; H, 4.28; N, 11.89. Found: C, 61.11; H, 4.21; N, 11.96.  $^1\text{H}$  NMR (300 MHz, DMSO- $d_6$ ):  $\delta$  2.69 (s, 3H), 7.18 (t,  $J$  = 7.29 Hz, 1H), 7.29-7.4 (m, 4H), 7.56 (d,  $J$  = 7.89 Hz, 2H), 7.67 (t,  $J$  = 7.2 Hz, 1H), 8 (d,  $J$  = 7.2 Hz, 1H), 10.27 (s, 1H), 15.66 (s, 1H).  $^{13}\text{C}$  NMR (75 MHz, DMSO- $d_6$ ) in ppm:  $\delta$  18.08, 49.07, 96.37, 116.76, 119.7, 123.93, 124.4, 125.38, 126.01, 129.14, 134.63, 139.32, 153.47, 161.89, 177.63, 179.24. IR ( $\text{cm}^{-1}$ ) in KBr: 3325  $\nu$ (O-H); 3223, 3157  $\nu$ (N-H); 3057, 2924  $\nu$ (C-H); 1660  $\nu$ (C=O, cyclic ester); 1605  $\nu$ (C=N); 1228  $\nu$ (C=S). HRMS: Calculated for

$C_{18}H_{16}N_3O_3S$  [M + H]<sup>+</sup> (m/z): 354.0912; found: 354.1246. UV-Vis (in CH<sub>3</sub>CN),  $\lambda_{max}$  ( $\epsilon$ , M<sup>-1</sup>cm<sup>-1</sup>): 327 (11255).

### **Synthesis of (E)-2-((1-methyl-1H-imidazol-2-yl)methylene)-N-phenylhydrazine-1-carbothioamide (HL<sup>3</sup>)**

To a methanolic solution (8 mL) of 1-methyl-2-imidazolecarbaldehyde (0.06 mL), 0.1 g (0.6 mmol) of 4-phenylthiosemicarbazide was added and heated for 3 h. The reaction mixture was filtered after the completion of the reaction and kept it for the slow evaporation of solvent. Needle shape colourless crystals appropriate for X-ray diffraction of the ligand were appeared. The yield was 0.12 g (78%).

Anal. Calc. for C<sub>12</sub>H<sub>13</sub>N<sub>5</sub>S: C, 55.58; H, 5.05; N, 27.01. Found: C, 55.65; H, 4.98; N, 27.03. <sup>1</sup>H NMR (400 MHz, DMSO-d<sub>6</sub>):  $\delta$  3.9 (s, 3H), 7.2 (t, J = 7.28 Hz, 1H), 7.31-7.38 (m, 4H), 7.62 (t, J = 8 Hz, 2H), 8.19 (s, 1H), 10.43 (s, 1H), 11.88 (s, 1H). <sup>13</sup>C NMR (75 MHz, DMSO-d<sub>6</sub>) in ppm:  $\delta$  33.53, 123.57, 124.37, 125.45, 125.59, 125.81, 128.59, 128.65, 128.82, 139.31, 140.99, 176.82. IR (cm<sup>-1</sup>) in KBr: 3301, 3124,  $\nu$ (N-H); 3100, 3000, 2922,  $\nu$ (C-H); 1593  $\nu$ (C=N); 1192  $\nu$ (C=S). HRMS: Calculated for C<sub>12</sub>H<sub>14</sub>N<sub>5</sub>S [M + H]<sup>+</sup> (m/z): 260.0970; found: 260.1049. UV-Vis (in CH<sub>3</sub>CN),  $\lambda_{max}$  ( $\epsilon$ , M<sup>-1</sup>cm<sup>-1</sup>): 330 (30770), 246 (8735).

### **Synthesis of [Pd(HL<sup>1</sup>)Cl] (C1)**

0.06 g (0.338 mmol) of palladium chloride (PdCl<sub>2</sub>) was dissolved in acetonitrile by heating the solution and then it was added to the solution of H<sub>2</sub>L<sup>1</sup> (0.1 g, 0.338 mmol) in acetonitrile and refluxed the resulting mixture for 12 h. Then the mixture was cooled to r.t and filtered it. Red colour single crystals of the complex suitable for diffraction were obtained after few days by the slow evaporation of the solvent. The yield was 0.11 g (70 %).

Anal. Calc. for C<sub>17</sub>H<sub>13</sub>ClN<sub>4</sub>OSPd: C, 44.08; H, 2.83; N, 12.09; S, Found: C, 44.16; H, 2.90; N, 12.19. IR (KBr, cm<sup>-1</sup>): 3418  $\nu$ (O-H); 3347  $\nu$ (N-H); 3058  $\nu$ (C-H); 1531  $\nu$ (C=N); 760  $\nu$ (C-S). <sup>1</sup>H NMR (300 MHz, DMSO-d<sub>6</sub>):  $\delta$  7.01 (t, J = 7.14 Hz, 1H), 7.09-7.16 (m, 2H), 7.23-7.35 (m, 4H) 7.85 (d, J = 8.43 Hz, 1H), 8.34 (d, J = 8.78 Hz, 1H), 8.45 (s, 1H), 8.79 (d, J = 8.4 Hz, 1H), 9.76 (s, 1H), 10.43 (s, 1H). HRMS: Calculated for C<sub>17</sub>H<sub>13</sub>N<sub>4</sub>OSPd [M - Cl]<sup>+</sup> (m/z): 426.9845; found: 426.9903. UV-Vis (in CH<sub>3</sub>CN),  $\lambda_{max}$  ( $\epsilon$ , M<sup>-1</sup>cm<sup>-1</sup>): 391 (3045), 325 (2274), 250 (7370).

### **Synthesis of [Pd(L<sup>2</sup>)(PPh<sub>3</sub>)] (C2)**

PdCl<sub>2</sub> (0.05 g, 0.28 mmol) solution (in acetonitrile) was added to a solution of H<sub>2</sub>L<sup>2</sup> (0.1 g, 0.28 mmol) in acetonitrile and refluxed for 2 h and then PPh<sub>3</sub> (0.11 g, 0.42 mmol) was added to the reaction mixture and refluxed the resultant mixture for 5 h. Orange colour crystals of C2 were obtained after the evaporation of the solvent. The yield was, 0.14 g, 68%.

Anal. Calc. for C<sub>36</sub>H<sub>28</sub>N<sub>3</sub>O<sub>3</sub>SPPd: C, 60.05; H, 3.92; N, 5.84. Found: C, 60.14; H, 3.96; N, 5.92. IR (KBr, cm<sup>-1</sup>): 3345  $\nu$ (N-H); 3060, 2922, 2853  $\nu$ (C-H), 1691  $\nu$ (C=O, cyclic ester); 1600  $\nu$ (C=N); 744  $\nu$ (C-S). <sup>1</sup>H

NMR (300 MHz, DMSO- $d_6$ ):  $\delta$  2.75 (s, 3H) 6.63 (d,  $J = 7.56$  Hz, 1H), 6.88-6.95 (m, 2H), 7.22-7.31 (m, 4H), 7.47-7.71 (m, 17H) 9.56 (s, 1H). HRMS: Calculated for  $C_{36}H_{28}N_3O_3SPPd$  [ $M + H$ ] $^+$  ( $m/z$ ): 720.0702; found: 720.0710. UV-Vis (in  $CH_3CN$ ),  $\lambda_{max}$  ( $\epsilon$ ,  $M^{-1}cm^{-1}$ ): 372 (4018), 287 (sh.), 252 (sh.).

### Synthesis of $[Pd(L^3)(PPh_3)]Cl$ (**C3**)

The procedure for the synthesis of **C3** was same as **C2**, here ligand was **HL<sup>3</sup>** (0.07 g, 0.28 mmol). After the addition of  $PPh_3$ , orange red colour solution appear which was filtered and kept it for crystallization. Red colour crystals of **C3** were appeared after few days. Yield was 0.09 g (72 %).

Anal. Calc. for  $C_{30}H_{27}ClN_5SPPd$ : C, 57.47; H, 4.34; N, 11.17. Found: C, 57.58; H, 4.45; N, 11.25. IR (KBr,  $cm^{-1}$ ): 3345  $\nu(N-H)$ ; 3049, 2923, 2853  $\nu(C-H)$ , 1541  $\nu(C=N)$ ; 743  $\nu(C-S)$ .  $^1H$  NMR (300 MHz, DMSO- $d_6$ ):  $\delta$  3.94 (s, 3H), 7.08-7.73 (m, 4H), 8.5 (s, 1H), 10.3 (s, 1H). HRMS: Calculated for  $C_{30}H_{27}N_5SPPd$  [ $M - Cl$ ] $^+$  ( $m/z$ ): 626.0760; found: 625.9386. UV-Vis (in  $CH_3CN$ ),  $\lambda_{max}$  ( $\epsilon$ ,  $M^{-1}cm^{-1}$ ): 348 (8121), 257 (sh.).

### Procedure for the Suzuki Coupling Reaction

Aryl halide (1 mmol), phenylboronic acid (1 mmol),  $K_2CO_3$  (2 mmol) and catalyst (**C1/C2/C3**, 1 mol%) were mixed in 5 mL PEG 400 solvent and stirred under reflux condition (90° C) for 6-7 h. The product formation was primarily examined by TLC. Solvent was evaporated under reduced pressure after the completion of the reaction and the residue was poured in water and extracted using diethyl ether. The catalyst was separated and washed with diethyl ether. The diethyl ether part was dried using anhydrous sodium sulfate. Then the solvent was evaporated and the residue was purified by column chromatography on silica gel and identified by  $^1H$  NMR spectroscopy.

### Crystal structure determination and refinement

Details of crystal analysis, data collection and structure refinement data for **HL<sup>3</sup>**, **C1**, **C2** and **C3** are given in Table S1. The Bruker AXS D8 Quest CMOS diffractometer was used to acquire diffraction data using graphite monochromatized Mo-K $\alpha$  radiation ( $\lambda = 0.71073$ ) at 293°C and reflection data were recorded using the  $\omega$  scan technique. The SAINT program<sup>1</sup> was used to integrate the data, and SADABS<sup>2</sup> was used to make the absorption corrections. All data were polarization and Lorentz adjusted, and the non-hydrogen atoms were anisotropically refined. The refinement procedure took into account hydrogen atoms in accordance with the riding model. The structures were resolved by direct method and refined using SHELXL-2016/6 program<sup>3</sup> by full-matrix least-squares techniques.

### Theoretical study

Density functional theory (DFT) was used to optimize the complexes' full geometry using the B3LYP<sup>4</sup> hybrid exchange correlation functional. All elements except Pd were assigned with 6-31G(d) basis set while for Pd atoms LanL2dz<sup>5</sup> basis set with effective core potential was employed. On the optimized geometries, vibrational frequency calculations were done to make sure that each configuration is actually a local minimum on the potential energy surface. The Gaussian09 program<sup>6</sup> and the Gauss-

View, Version 5 visualization program were used for all calculations. Electronic transitions were calculated using the time-dependent density functional theory (TDDFT) formalism<sup>7</sup> using conductor-like polarizable continuum model (CPCM)<sup>8</sup> in acetonitrile to simulate the solvent. The fractional contributions of various groups to each molecular orbital were calculated using GaussSum.<sup>9</sup>

### **DNA interaction studies**

The binding experiments of metal complexes with calf thymus (CT) DNA were performed in Tris HCl/50 mM NaCl buffer (pH 7.4). A stock solution of CT DNA was prepared in that buffer and the concentration of the CT DNA was determined by dividing its absorption value at 260 nm with the molar extinction coefficient value i.e., 6600 M<sup>-1</sup> cm<sup>-1</sup>.<sup>55</sup> The stock solution of the complexes was prepared in DMSO medium ( $\sim 10^{-4}$  M) and was suitably diluted with Tris buffer whenever necessary. By keeping constant concentration of complexes, absorption titration was carried out by gradually adding the CT DNA solution. The competitive studies of the complexes with ethidium bromide (EB) were investigated with fluorescence spectroscopy in order to examine whether the compound can displace EB from its EB-CT DNA complex. The EB-CT DNA adduct was prepared by adding 15  $\mu$ M EB and 30  $\mu$ M CT DNA in buffer (Tris-HCl/NaCl buffer at pH 7.4). The influence of the addition of the complexes to the EB-CT DNA adduct solution has been obtained by recording the emission spectra and the observed quenching is attributed to the displacement of EB from its EB-CT DNA adduct.

The viscosity of the CT-DNA solution (30  $\mu$ M) was measured by increasing the concentration of the complexes using an Ostwald viscometer placing in a thermostated water bath at 20.0 °C. Flow time has been measured three times for each concentration of the compound and then the average flow time was calculated. Viscosity values were calculated from the observed flow time of DNA-containing solutions ( $t$ ) corrected for the flow time of buffer alone ( $t_0$ ),  $\eta = t - t_0$ . The data is reported as  $(\eta / \eta_0)^{1/3}$  versus the ratio of the concentration of the compound to CT-DNA ( $R$ ), where  $\eta$  is the viscosity of CT-DNA in the presence of the compound and  $\eta_0$  is the viscosity of CT-DNA solution alone.

### **BSA protein binding studies**

It was feasible to ascertain how the BSA protein interacted with the complexes by measuring absorption and emission. In order to do this, a BSA stock solution (5  $\mu$ M) in 500 mM phosphate buffer saline (PBS) at pH 7.4 was produced and stored at 4°C in the dark. The complex solutions ( $\sim 10^{-4}$  M) were prepared in DMSO solvent and was suitably diluted with PBS whenever necessary. During the absorption titration tests, the addition concentrations of the complexes were varied while the BSA (5  $\mu$ M) concentration was maintained constant. Similarly, fluorescence titrations were performed with a fixed BSA concentration. A micropipette was used to manually add the compounds to both the absorbance and emission titrations.

## CD spectral study

Circular dichroism (CD) measurements were obtained by employing JASCO (J-815) spectropolarimeter at 298 K using a quartz cuvette of 1 cm cell path length. The spectra were carried out by keeping a constant BSA concentration (0.48  $\mu\text{M}$ ) and the spectra were recorded in the absence and presence of the three complexes. The CD results were expressed in terms of the mean residual ellipticity (MRE) in  $\text{deg cm}^2 \text{dmol}^{-1}$  according to the following equation (eq 1).

$$\text{MRE} = \text{observed CD (mdeg)} / 10C_p n l \quad (1)$$

Where,  $C_p$  represents the molar concentration of the protein,  $n$  stands for the number of amino acid residues (583 for BSA) and  $l$  is the path length of the cell (1 cm). The  $\alpha$ -helical (%) contents of the free and bound BSA were calculated from the mean MRE values at 208 nm using the following equation (eq 2).

$$\alpha\text{-helix (\%)} = [(-\text{MRE}_{208} - 4000) / (33,000 - 4000)] \times 100 \quad (2)$$

Where,  $\text{MRE}_{208}$  is the MRE value observed at 208 nm, 4000 is the MRE of the  $\beta$ -form and random coil conformation at 208 nm, and 33000 is the MRE value of a pure  $\alpha$ -helix at 208 nm.

## Förster Resonance Energy Transfer (FRET)

The value of  $R_0$  was calculated using equation (3).

$$R_0 = 0.2018 \{[\kappa^2 \phi_D \eta^{-4} J(\lambda)]^{1/6}\} \text{ \AA} \quad (3)$$

where the orientation factor between the emission dipole of the donor and the absorption dipole of the acceptor  $\kappa^2$  is taken as 2/3, the fluorescence quantum yield of the donor  $\phi_D$  is 0.118, the refractive index of the medium ( $\eta$ ) is 1.33, and  $J(\lambda)$  is the extent of spectral overlap of donor (BSA) emission and the acceptor (complex) absorption spectra.<sup>10</sup> The value of  $J(\lambda)$  can be calculated using eqn (4).<sup>11</sup>

$$J(\lambda) = \int_0^{\infty} \bar{I}_D(\lambda) \varepsilon_A(\lambda) \lambda^4 d\lambda \quad M^{-1} \text{cm}^{-1} \text{nm}^4 \quad (4)$$

Where,  $\bar{I}_D(\lambda)$  denotes the normalized fluorescence emission of the donor BSA at the wavelength  $\lambda$ , and  $\varepsilon_A(\lambda)$  represents the molar extinction coefficient of the acceptor metal complex at the wavelength  $\lambda$ .

## In Vitro Cytotoxicity Study

### Cell culture

The human breast adenocarcinoma (MDA-MB-231) cell line was obtained from the National Centre for Cell Science (NCCS) in Pune, India. The cells were cultured in Dulbecco's modified Eagle's medium (DMEM) with high glucose, supplemented with 10% heat-inactivated fetal bovine serum (FBS) from Gibco™, USA, and 1% Penicillin-Streptomycin (Gibco™, USA). The cell culture was maintained in a

5% CO<sub>2</sub> atmosphere at 37°C in a humidified incubator. When the cells reached approximately 70-80% confluency, they were harvested using a 0.25% Trypsin-EDTA (Gibco™, USA) solution and then seeded at an appropriate density to allow them to re-equilibrate before the start of the experiment. This process ensures that the cells are in a suitable state for subsequent experimental procedures.

### **Cell viability assay**

To determine cell viability, the MTT [(4,5-dimethyl-thiazol-2-yl)-2,5-diphenyl tetrazolium bromide] assay was performed using MTT reagent obtained from Sigma Aldrich, USA. In this assay, MDA-MB-231 cells were seeded in a 96-well plate at a density of 10,000 cells per well. The cells were then treated with different concentrations of **C3** (0, 5, 10, 15, 20, 25, 30, 35, 40, 45, and 50 μM). After the treatment, the plates were incubated for 24 hours at 37°C in a humidified CO<sub>2</sub> (5%) incubator. Following the incubation period, the cells were washed thoroughly with phosphate-buffered saline (PBS). Subsequently, MTT solution with a concentration of 4 mg/mL was added to each well, and the plates were returned to the incubator for 4 hours. After the incubation with MTT, the intracellular formazan salt formed was solubilized by adding dimethyl sulfoxide (DMSO). Cell viability was assessed using absorbance measurements to determine cell proliferation. The absorbance values were used to calculate cell viability using the formula:  $\text{Cell viability (\%)} = (\text{OD}_{\text{control}} - \text{OD}_{\text{sample}}) / \text{OD}_{\text{control}} \times 100$ . In this formula, OD<sub>control</sub> represents the absorbance of untreated cells, while OD<sub>sample</sub> represents the absorbance of treated cells. To ensure the reliability of the results, the experiments were conducted multiple times, allowing for the reduction of experimental variability and ensuring the consistency and reproducibility of the findings. The absorbance of the solubilized formazan salt was measured at 595 nm using an ELISA reader (EMax, Molecular Device, USA). This measurement provided an indication of cell viability, as the intensity of the absorbance was proportional to the number of viable cells in each well.

### **Quantification of apoptosis using flow cytometry**

To analyze apoptosis, flow cytometry was performed using the Dead Cell Apoptosis Kit with Annexin V obtained from Invitrogen™, USA.<sup>60-62</sup> Treated cells at a density of  $1 \times 10^6$  were harvested and stained with Annexin-V-FITC and propidium iodide (PI) following the manufacturer's instructions. The staining procedure involved the labeling of cells with Annexin-V-FITC, which binds to phosphatidylserine exposed on the outer membrane of apoptotic cells. PI was used to stain cells with compromised cell membranes, such as necrotic cells. The staining allowed for the differentiation of viable, apoptotic (early and late), and necrotic cells. After staining, flow cytometry analysis was performed using a BD LSRFortessa flow cytometer (San Jose, CA, USA). The flow cytometer measured the fluorescence emitted by Annexin-V-FITC and PI to determine the proportions of viable, apoptotic, and necrotic cells within the cell population. This analysis provided

quantitative information about the induction of apoptosis and the extent of cell death in the treated cell samples.

#### **Measurement of mitochondrial membrane potential using flow cytometry**

For assessing mitochondrial membrane potential, treated cells were incubated with JC-1, a cationic carbocyanine dye obtained from Invitrogen™, USA. The dye accumulates in the mitochondria in a potential-dependent manner. It undergoes a fluorescence emission shift from green (525 nm) to red (590 nm) when the mitochondrial membrane potential is intact. After incubation with JC-1, flow cytometric analysis was performed following the manufacturer's protocol. The flow cytometer measured the fluorescence emitted by JC-1 monomers and aggregates, allowing the determination of the percentage of depolarized and hyperpolarized mitochondria within the cell population. Depolarized mitochondria exhibit a decreased red/green fluorescence ratio, indicating a loss of mitochondrial membrane potential, while hyperpolarized mitochondria display an increased red/green fluorescence ratio, indicating intact mitochondrial membrane potential. By analyzing the fluorescence changes of JC-1, the flow cytometry data provided information about the mitochondrial membrane potential status in the treated cells, allowing the assessment of mitochondrial dysfunction or perturbation induced by the experimental treatment.

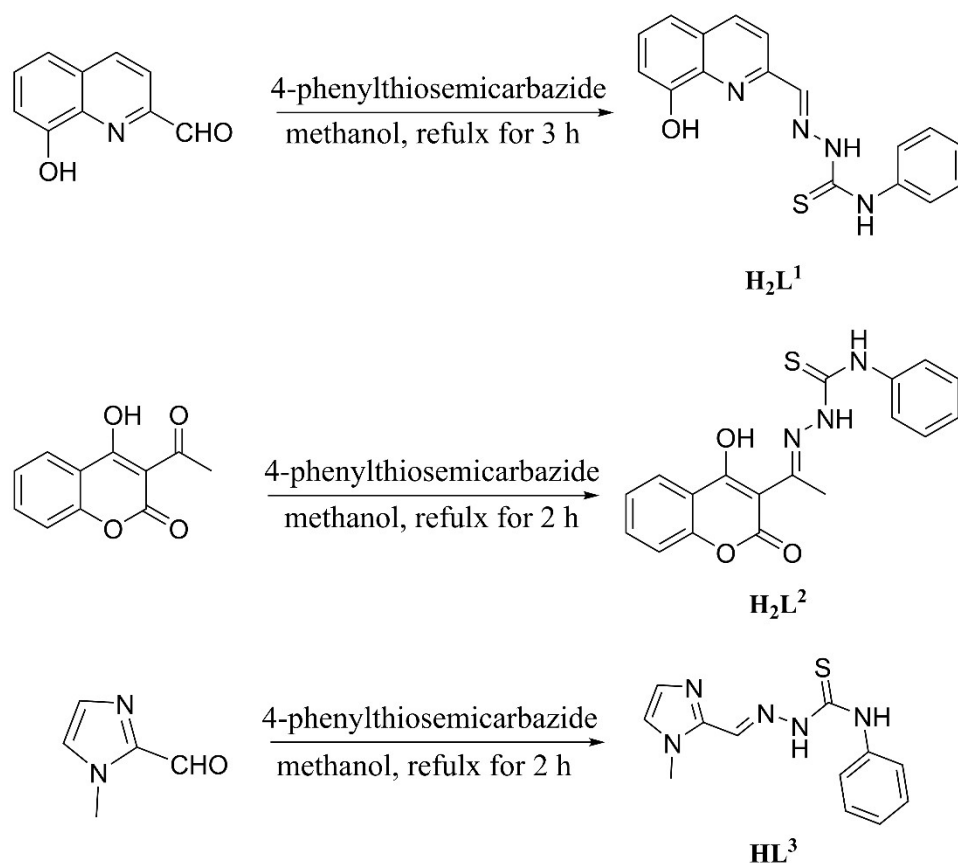
#### **Determination of intracellular ROS (iROS)**

To investigate the production of reactive oxygen species (ROS) within the treated cells, we utilized the fluorescent probe 2',7'-dichlorofluorescein diacetate (H<sub>2</sub>DCFH-DA) obtained from Invitrogen™. H<sub>2</sub>DCFH-DA is a non-fluorescent compound that can enter the cells and be converted into the fluorescent molecule 2',7'-dichlorofluorescein (DCF) in the presence of ROS. The treated cells were incubated with 10 mM H<sub>2</sub>DCFH-DA at 37 °C for 25 minutes. During this incubation period, the H<sub>2</sub>DCFH-DA was taken up by the cells and intracellularly converted to DCF in the presence of ROS. The intensity of DCF fluorescence directly reflects the level of ROS generated inside the cells. After incubation, the cells were analyzed using a flow cytometry (BD LSRFortessa, Becton Dickinson, Franklin Lakes, NJ, USA). The mean fluorescence intensity of DCF was measured, providing a quantitative assessment of intracellular ROS levels. The increment in DCF fluorescence intensity correlates with an increase in ROS production, indicating oxidative stress within the cells. This analysis allows us to evaluate the impact of the treatment on ROS generation and provides insights into the cellular response to oxidative stress induced by the experimental conditions.

#### **Confocal microscopy**

To examine the expression of apoptotic markers, including Caspase-3, Casase-9, Cytochrome C, BCL-2, p53, and p21, confocal microscopy was performed. The following steps were carried out: Control and treated MDA-MB-231 cells were washed twice with PBS (0.01 M) for 5 minutes each to remove

any residual media or reagents. The cells were then fixed with a 4% Paraformaldehyde solution in PBS and incubated for 15 minutes at room temperature. This fixation step helps preserve the cellular structure. After fixation, the cells were incubated in a blocking solution containing 2% normal bovine serum and 0.3% Triton X-100 in PBS for 1 hour. Blocking helps reduce nonspecific binding of antibodies and enhances the specificity of the staining. Following the blocking step, the cells were incubated overnight at 4 °C with the respective primary antibodies targeting Caspase-3, Casase-9, Cytochrome C, BCL-2, p53, and p21. These primary antibodies (obtained from CST, USA) specifically bind to their respective targets within the cells. After the overnight incubation, the cells were washed to remove unbound primary antibodies and then incubated with fluorophore-conjugated secondary antibodies for 4 hours. The secondary antibodies, such as anti-mouse/rabbit/goat Alexa Fluor-555, Alexa Fluor-647, and Alexa Fluor-488 (obtained from CST, USA), bind to the primary antibodies and enable visualization of the target proteins. To visualize the cell nuclei, the stained cells were counterstained with 6-diamidino-2-phenylindole (DAPI) obtained from Sigma, USA, for 5 minutes. DAPI binds to DNA, highlighting the nuclei of the cells. Finally, the slides containing the stained cells were mounted using Fluorescent Mounting Media, Aqueous obtained from Sigma, USA. This mounting media helps preserve the fluorescence and protect the slides. The stained cells were examined using a confocal laser scanning microscope (ZEISS LSM-980, Germany). The microscope allows the visualization of fluorescence signals with high resolution and the collection of optical sections through the cells. The acquired images were analyzed using ZEN 3.4 Blue edition software, which enables the quantification and analysis of the fluorescence signals from the different channels. This analysis helps determine the localization and expression levels of the apoptotic markers within the cells. By performing confocal microscopy and image analysis, we can gain insights into the spatial distribution and expression patterns of the apoptotic markers, providing valuable information about the cellular response to the treatment.



**Scheme S1:** Synthesis routes of the ligands **H<sub>2</sub>L<sup>1</sup>**, **H<sub>2</sub>L<sup>2</sup>** and **HL<sup>3</sup>**

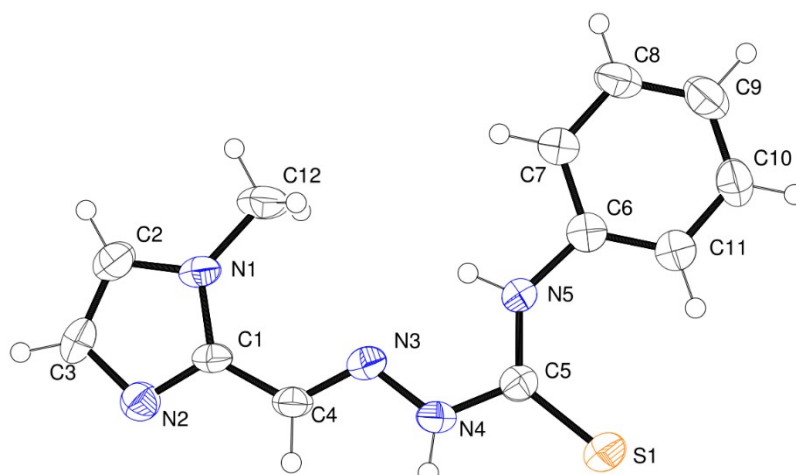


**Figure S1:** ORTEP view of ligand **HL<sup>3</sup>** with 50% ellipsoidal probability

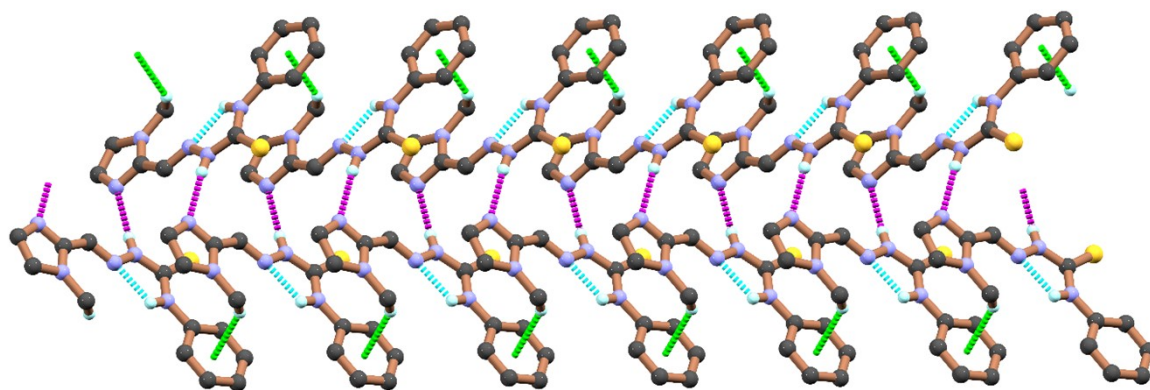


**Figure S2:** 2D supramolecular arrangement of ligand **HL<sup>3</sup>** formed by N5–H5···N3 hydrogen bond [2.08 Å, intramolecular; sky-blue color], N4–H4···N2 hydrogen bond [2.14 Å, intermolecular; purple color] and C–H··· $\pi$  interactions [2.744 Å, symmetry:  $-1+X, Y, Z$ ; green color].

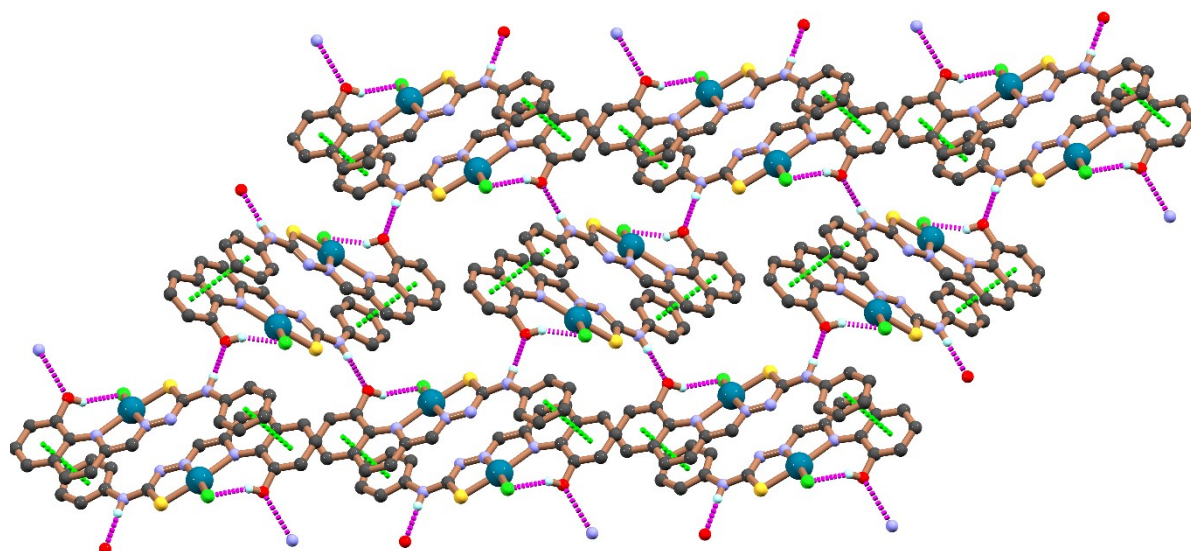


**Figure S3:** 3D architecture of **C1** shows hydrogen bonds (purple color) and  $\pi$ ··· $\pi$  interactions (green color).

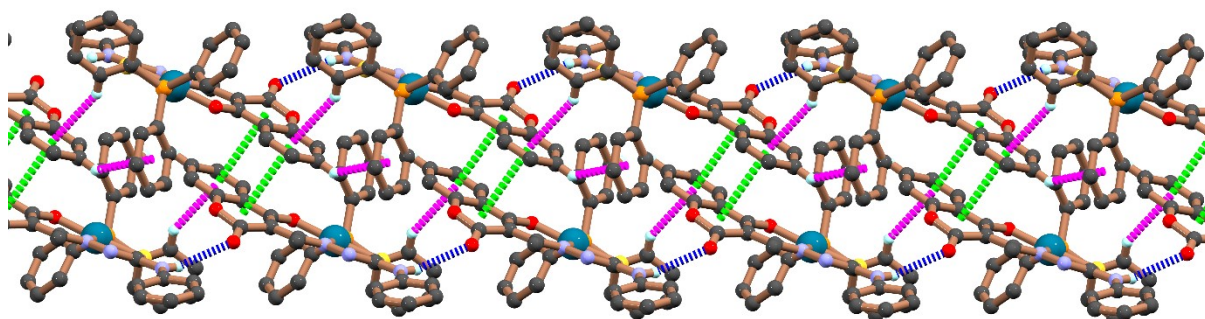


**Figure S4:** 3D supramolecular aggregate of **C2** along 'b' axis, constructed by hydrogen bond (blue color), C–H··· $\pi$  interactions (purple color) and  $\pi$ ··· $\pi$  interactions (green color).

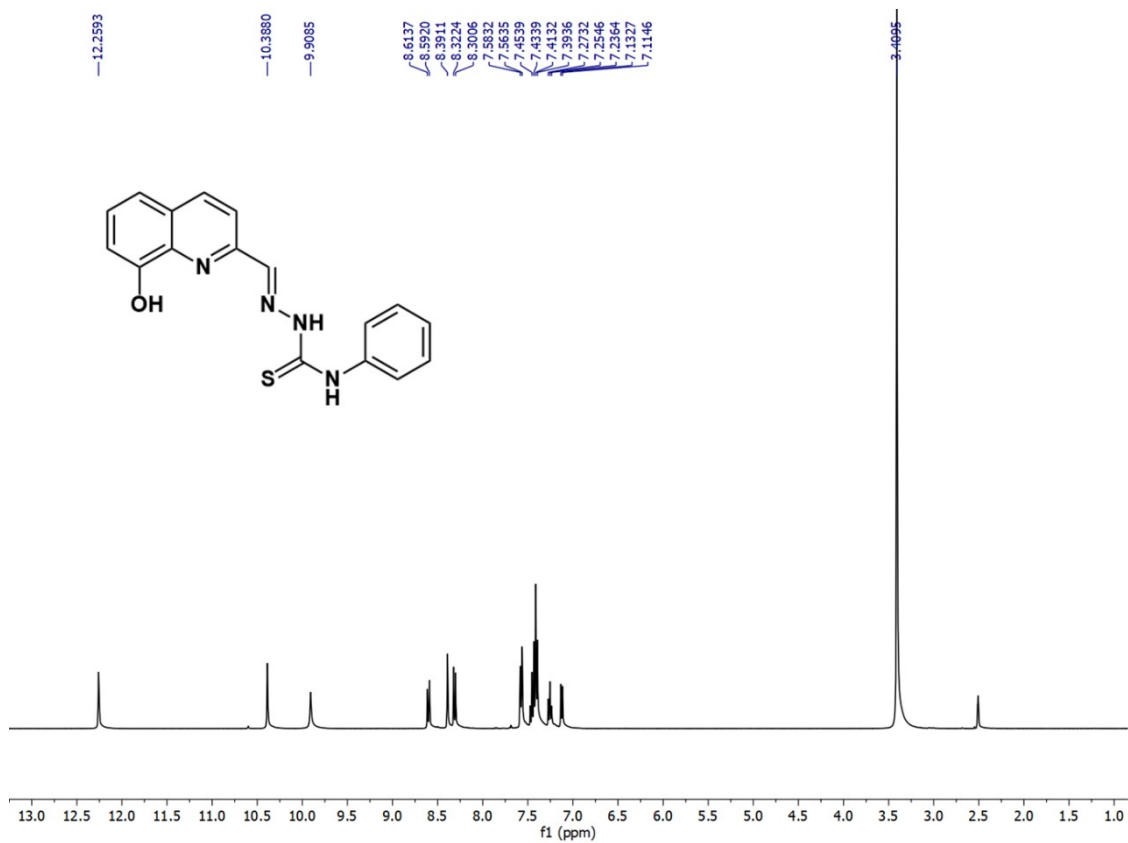


Figure S5:  $^1H$ -NMR spectrum of  $H_2L^1$  in  $DMSO-d_6$

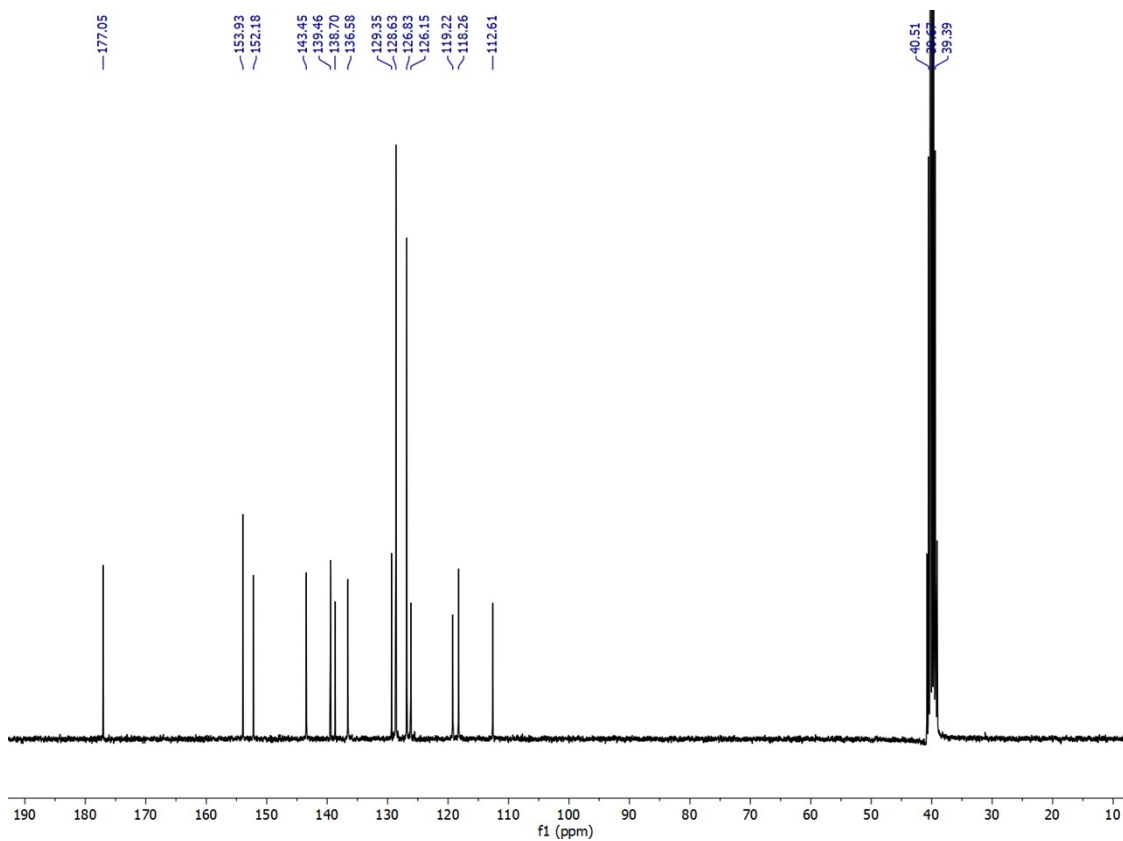


Figure S6:  $^{13}\text{C}$ -NMR spectrum of  $\text{H}_2\text{L}^1$  in  $\text{DMSO-d}_6$

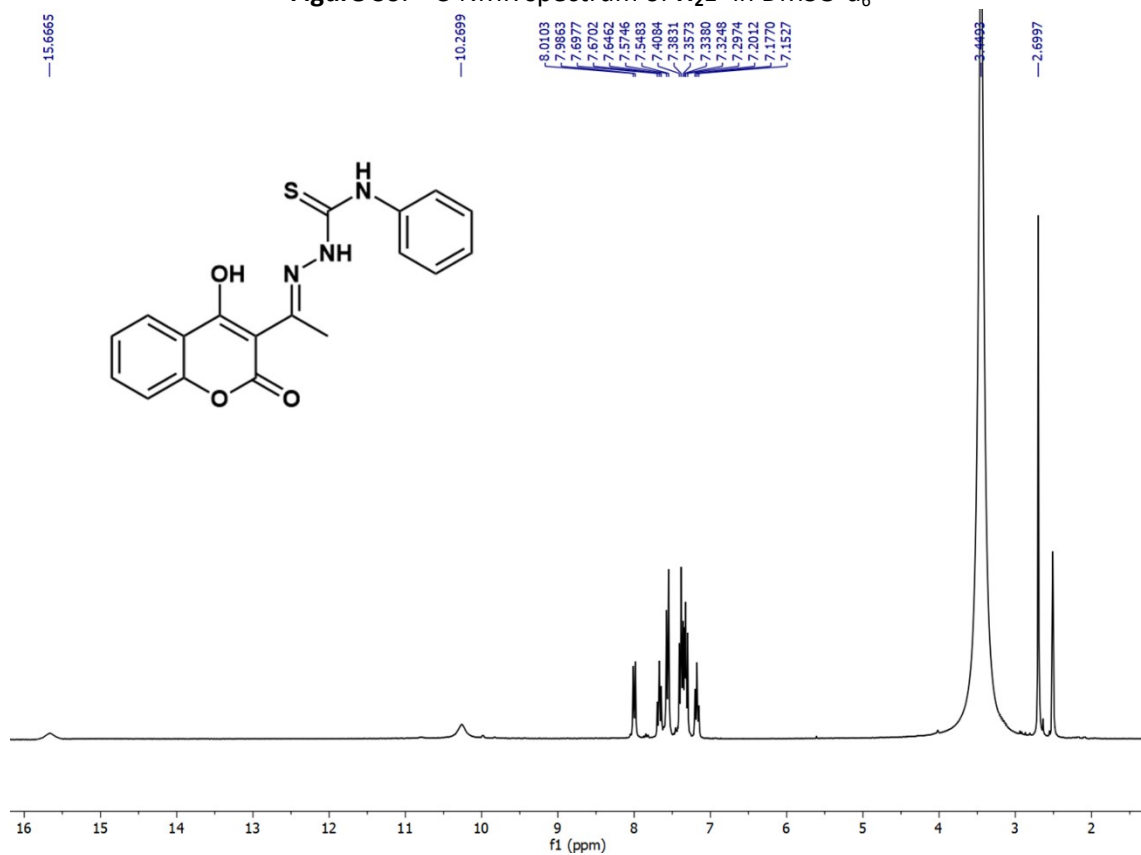


Figure S7:  $^1\text{H}$ -NMR spectrum of  $\text{H}_2\text{L}^2$  in  $\text{DMSO-d}_6$

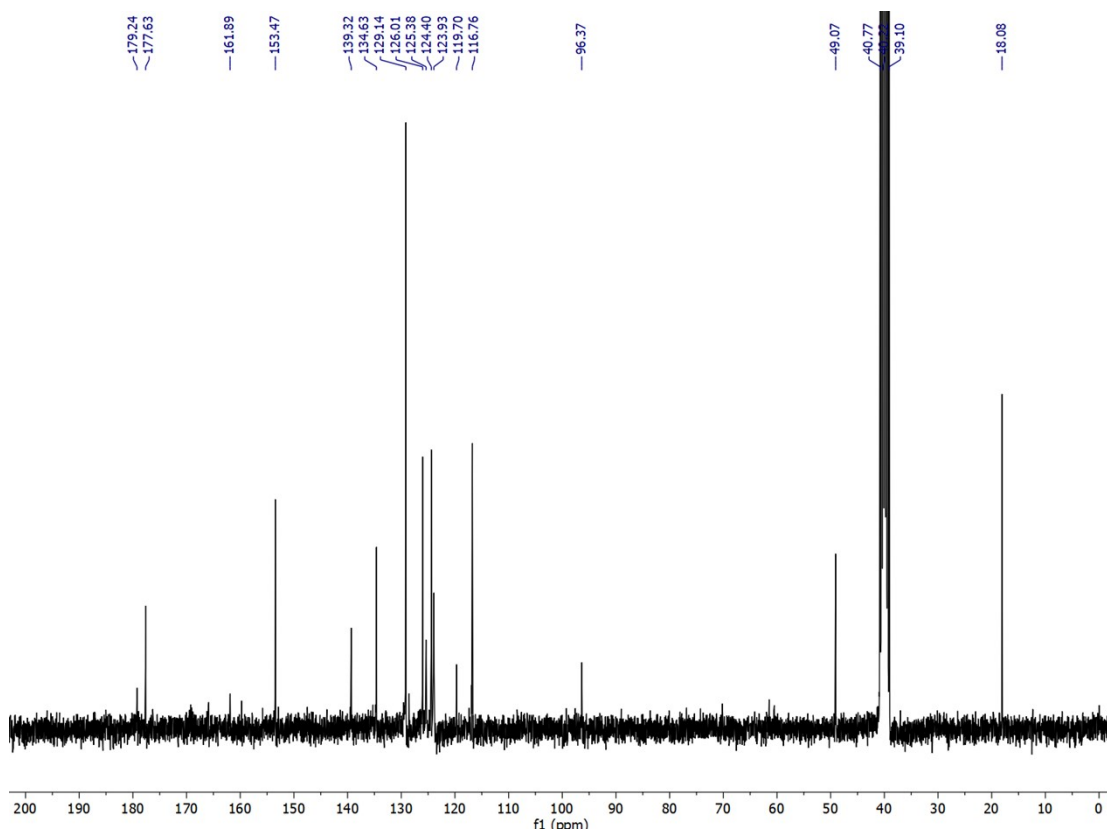


Figure S8:  $^{13}\text{C}$ -NMR spectrum of  $\text{H}_2\text{L}^2$  in  $\text{DMSO-d}_6$

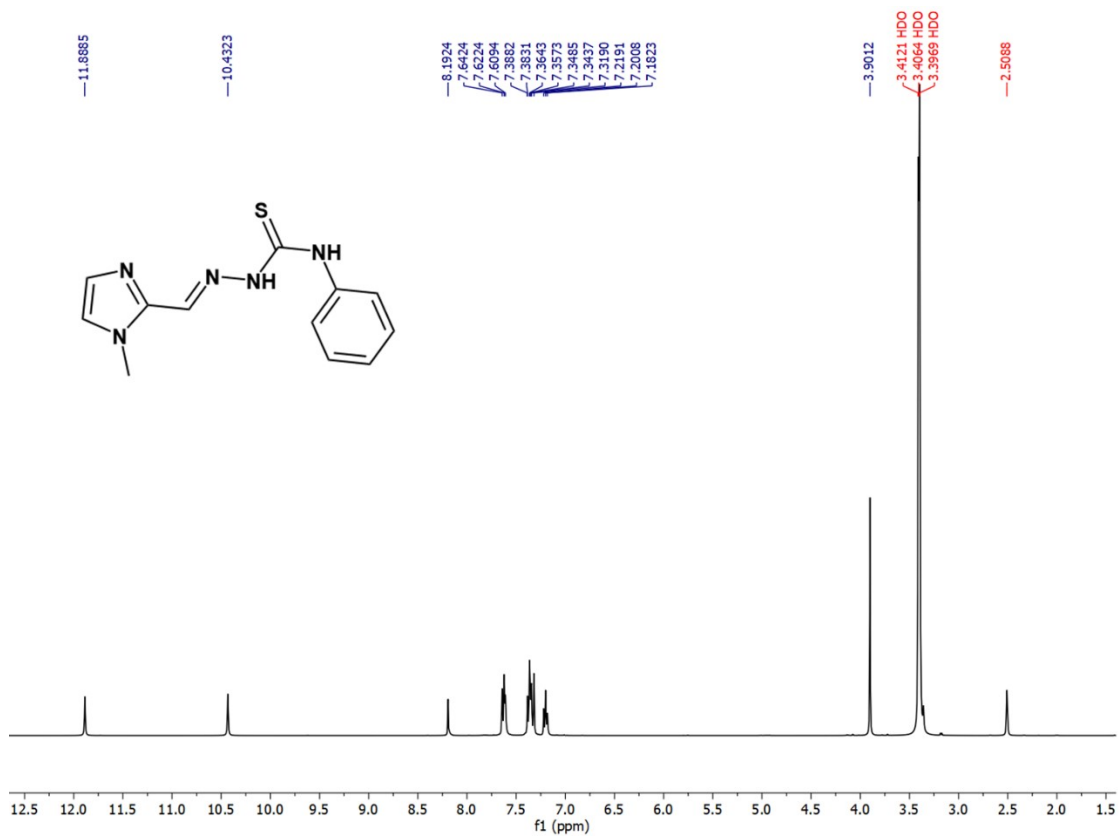


Figure S9:  $^1\text{H}$ -NMR spectrum of  $\text{HL}^3$  in  $\text{DMSO-d}_6$

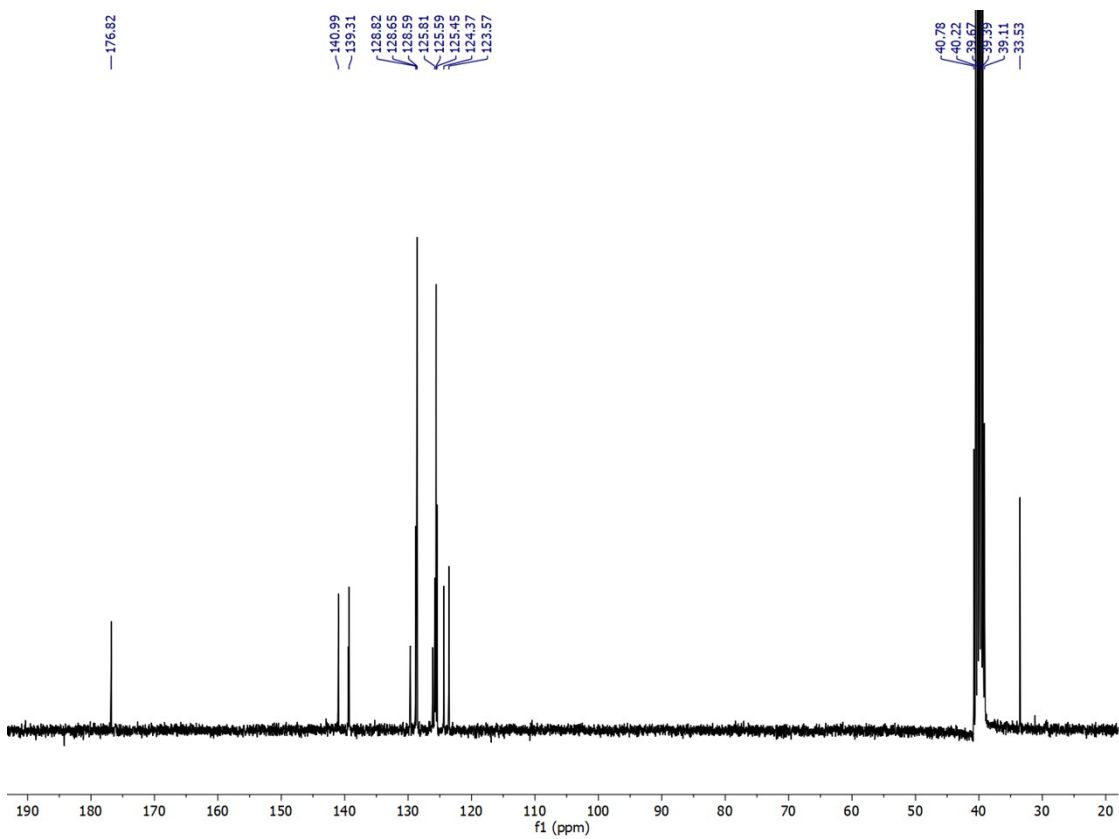


Figure S10:  $^{13}\text{C}$ -NMR spectrum of HL<sup>3</sup> in DMSO- $d_6$

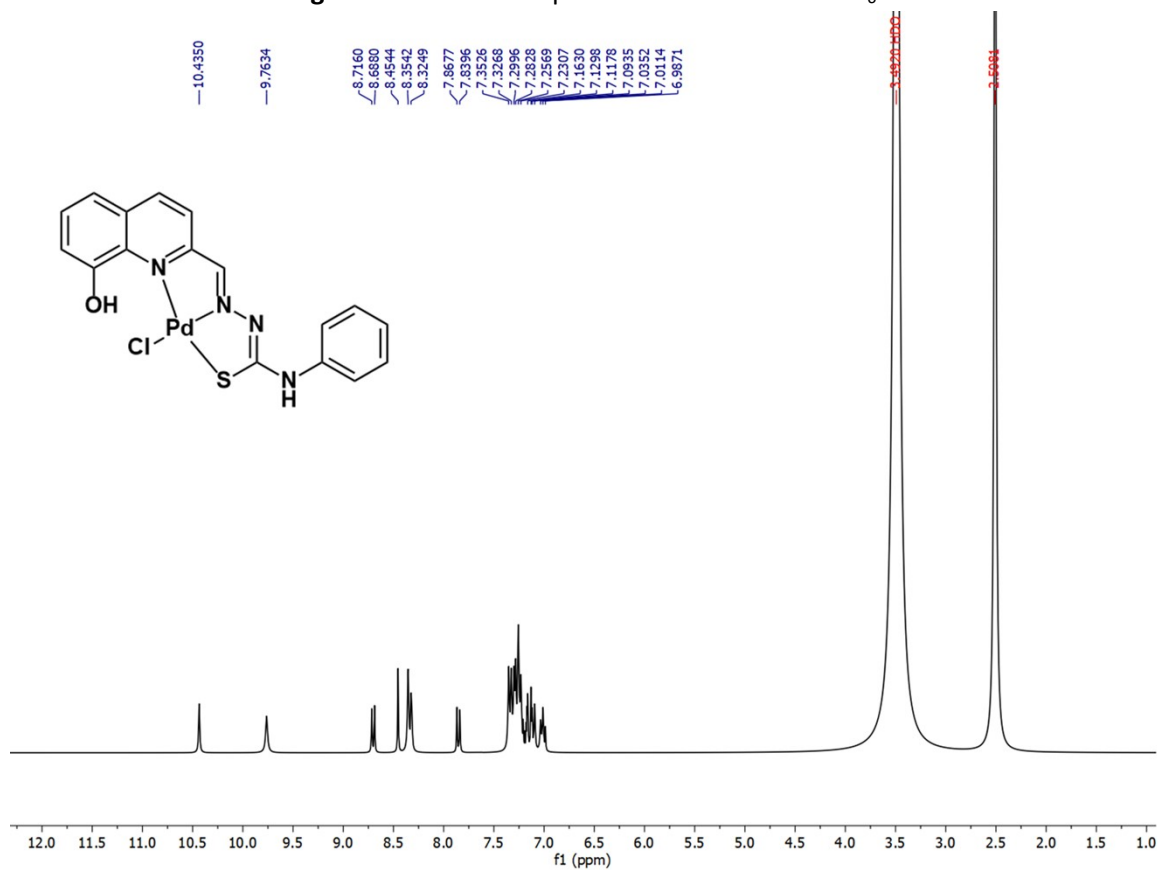


Figure S11:  $^1\text{H}$ -NMR spectrum of C1 in DMSO- $d_6$

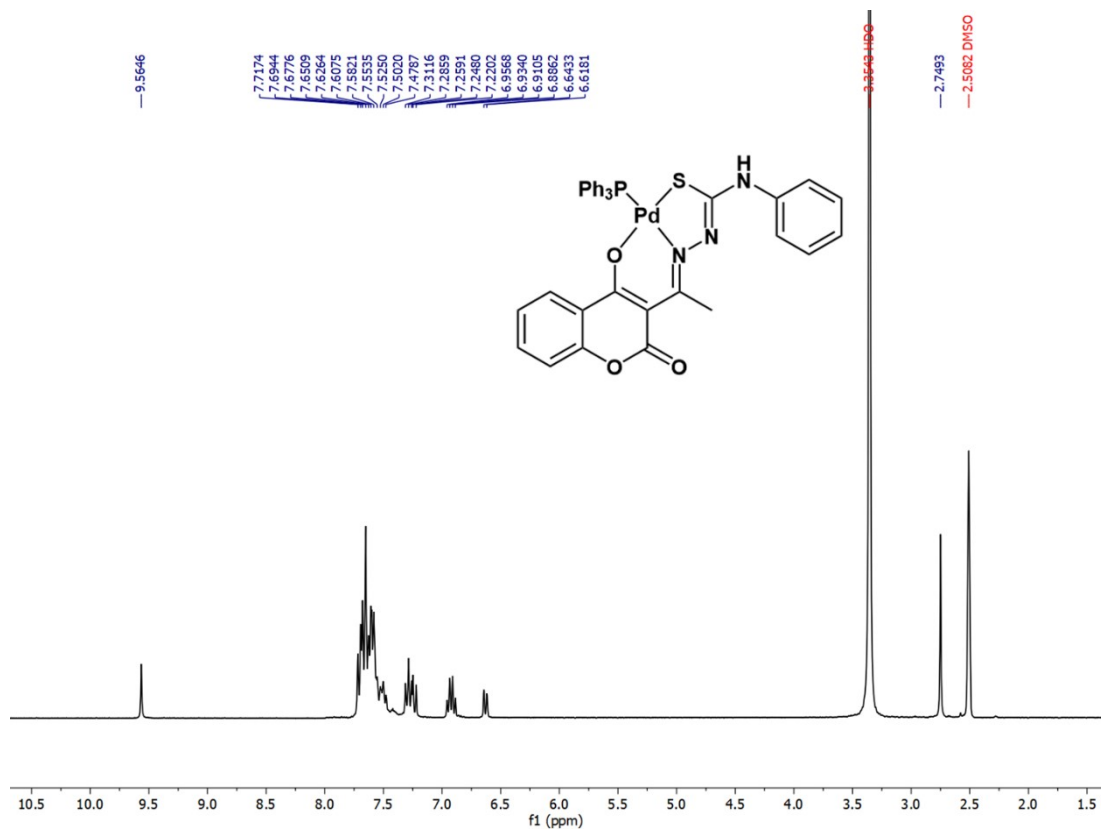


Figure S12:  $^1\text{H-NMR}$  spectrum of **C2** in  $\text{DMSO-d}_6$

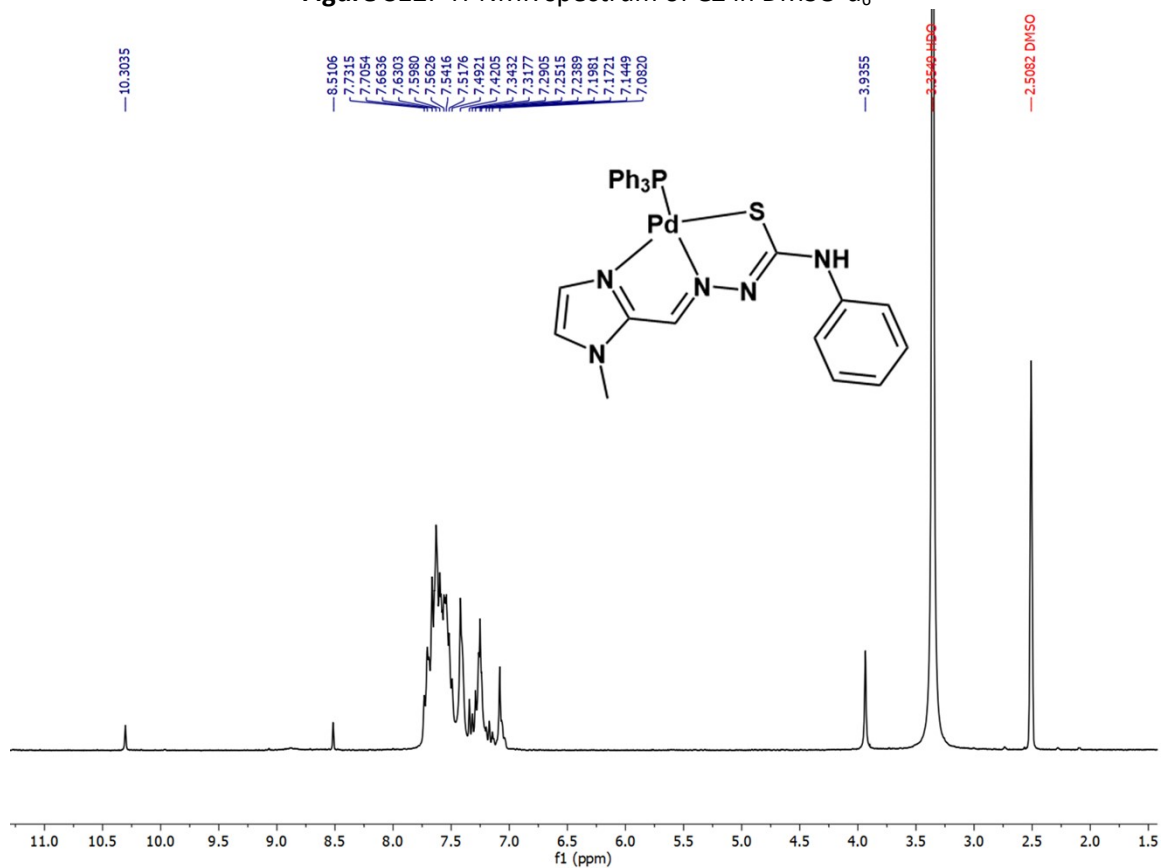


Figure S13:  $^1\text{H-NMR}$  spectrum of **C3** in  $\text{DMSO-d}_6$

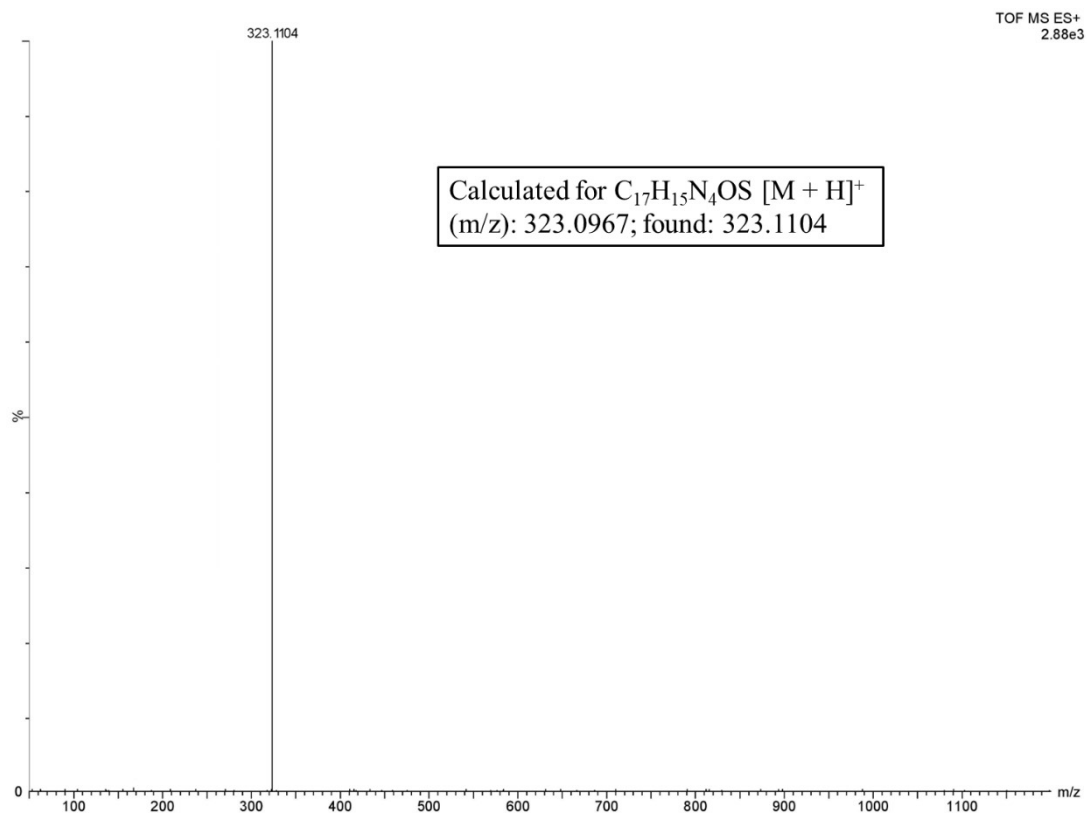


Figure S14: HRMS of H<sub>2</sub>L<sup>1</sup> in acetonitrile

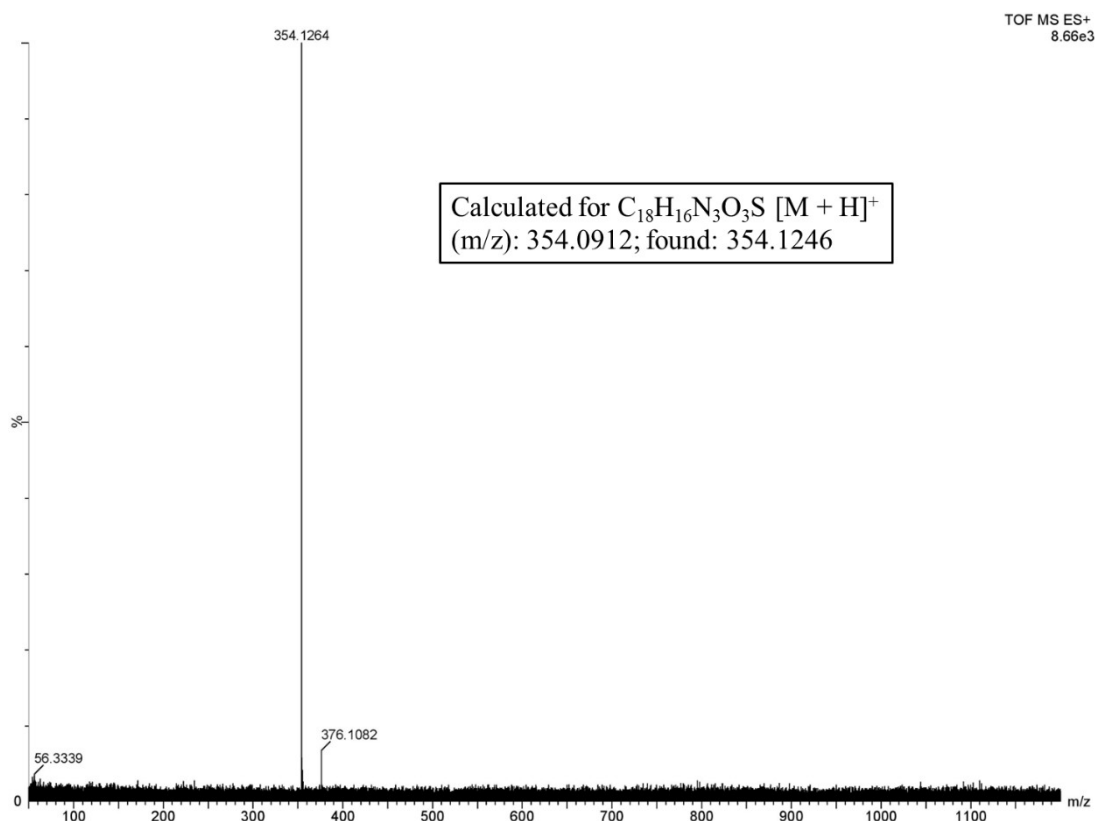


Figure S15: HRMS of H<sub>2</sub>L<sup>2</sup> in acetonitrile

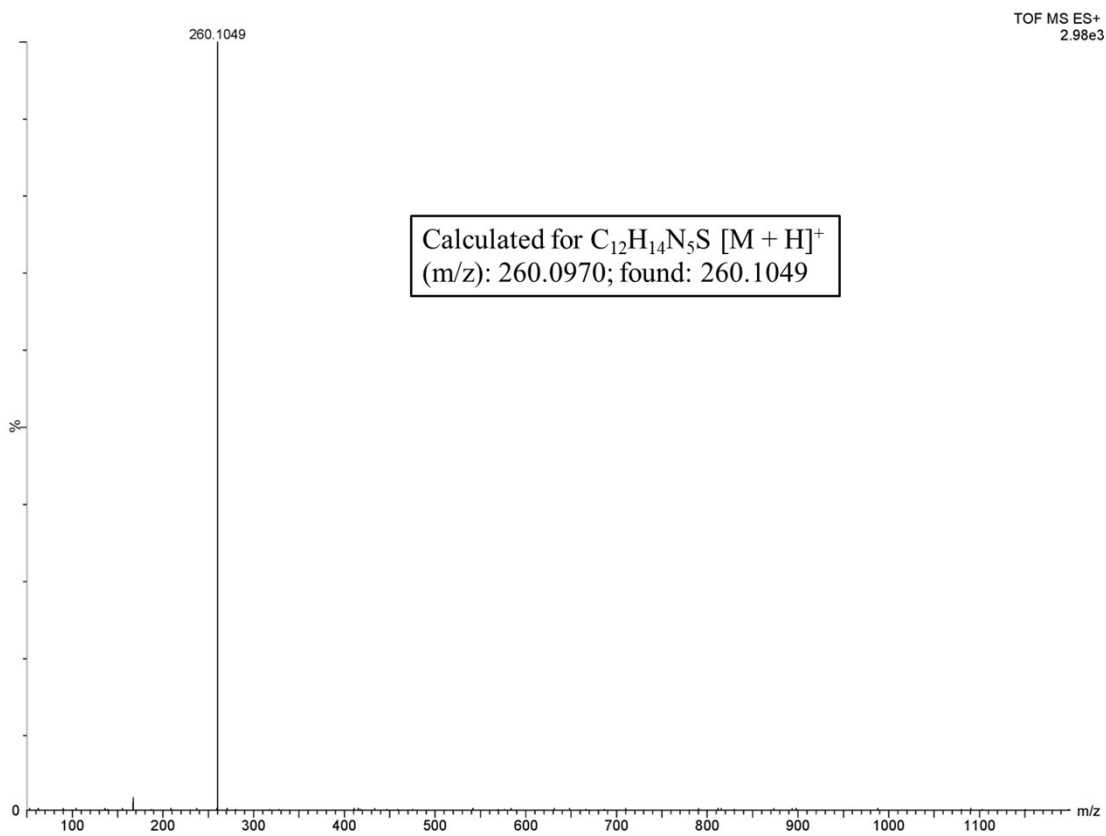


Figure S16: HRMS of HL<sup>3</sup> in acetonitrile

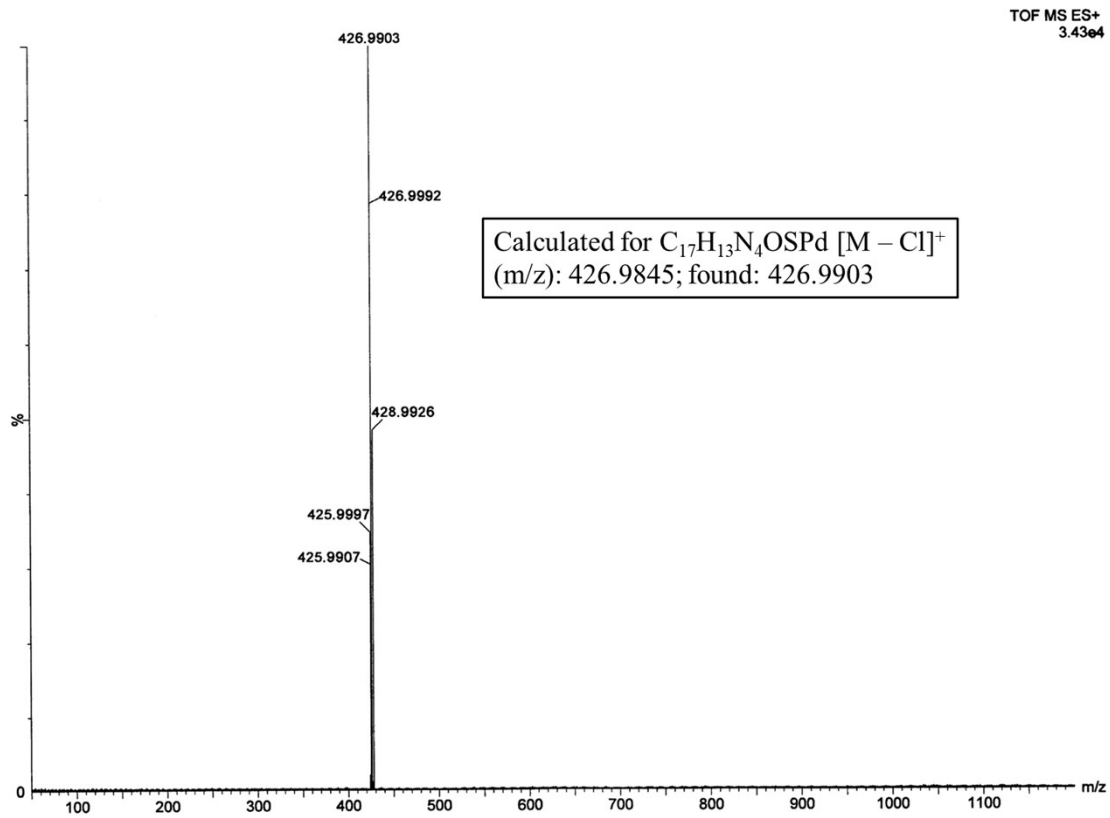


Figure S17: HRMS of C1 in acetonitrile

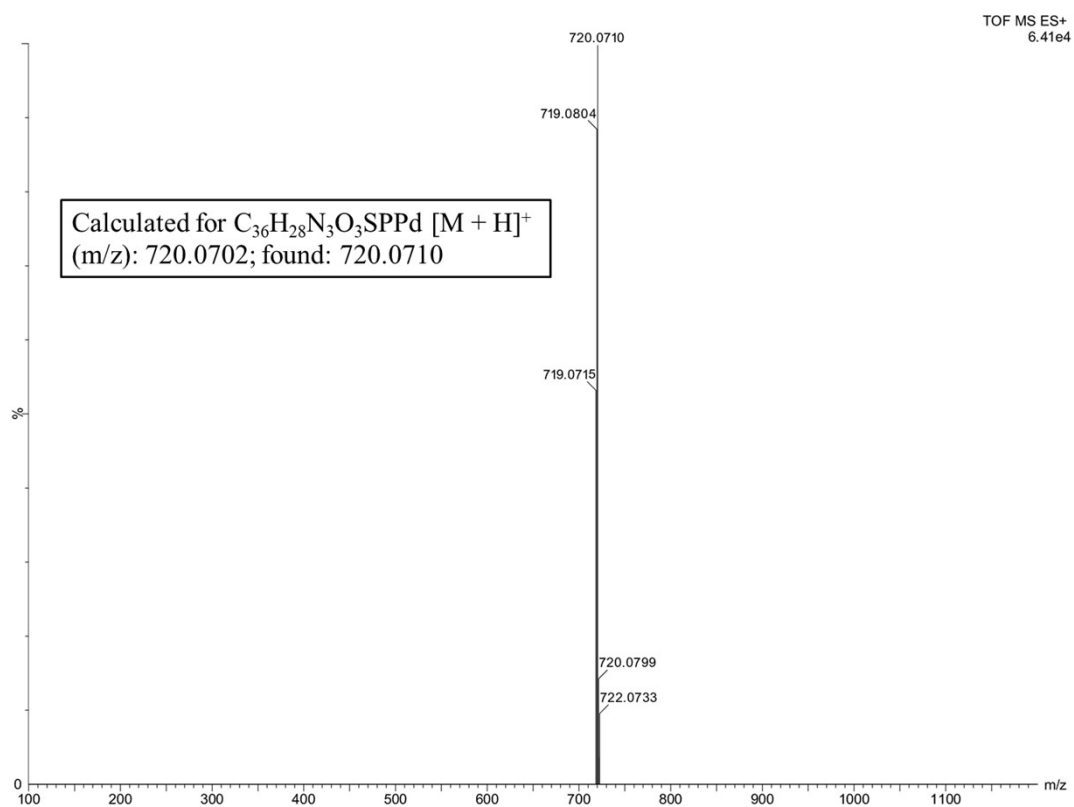


Figure S18: HRMS of C2 in acetonitrile

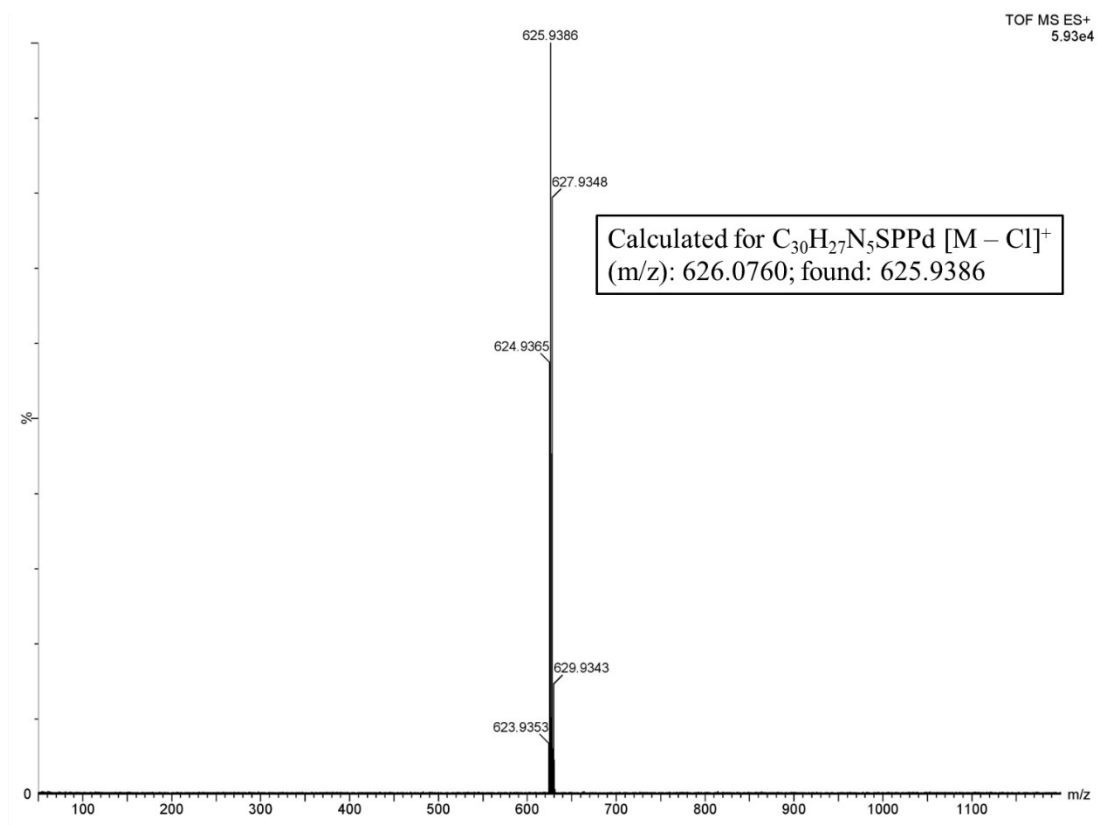
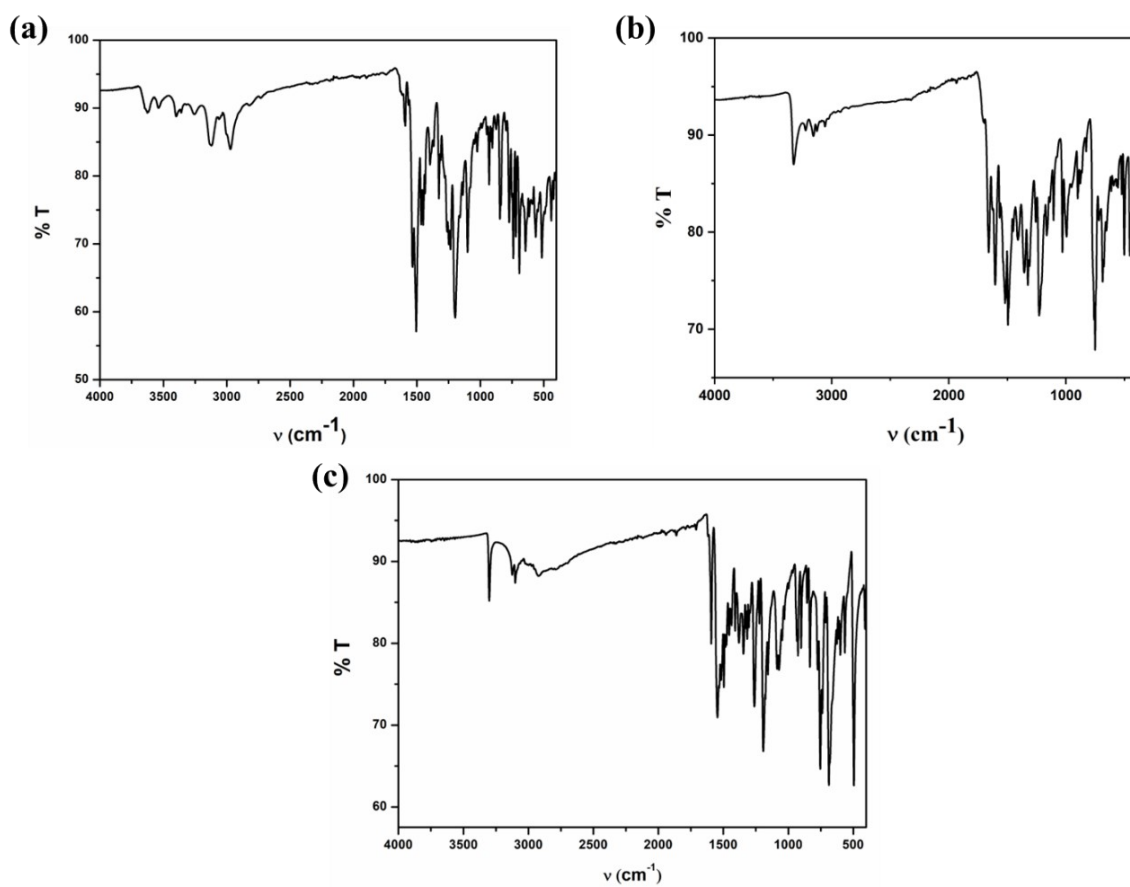


Figure S19: HRMS of C3 in acetonitrile



**Figure S20:** IR spectra of (a)  $H_2L^1$ , (b)  $H_2L^2$  and (c)  $HL^3$

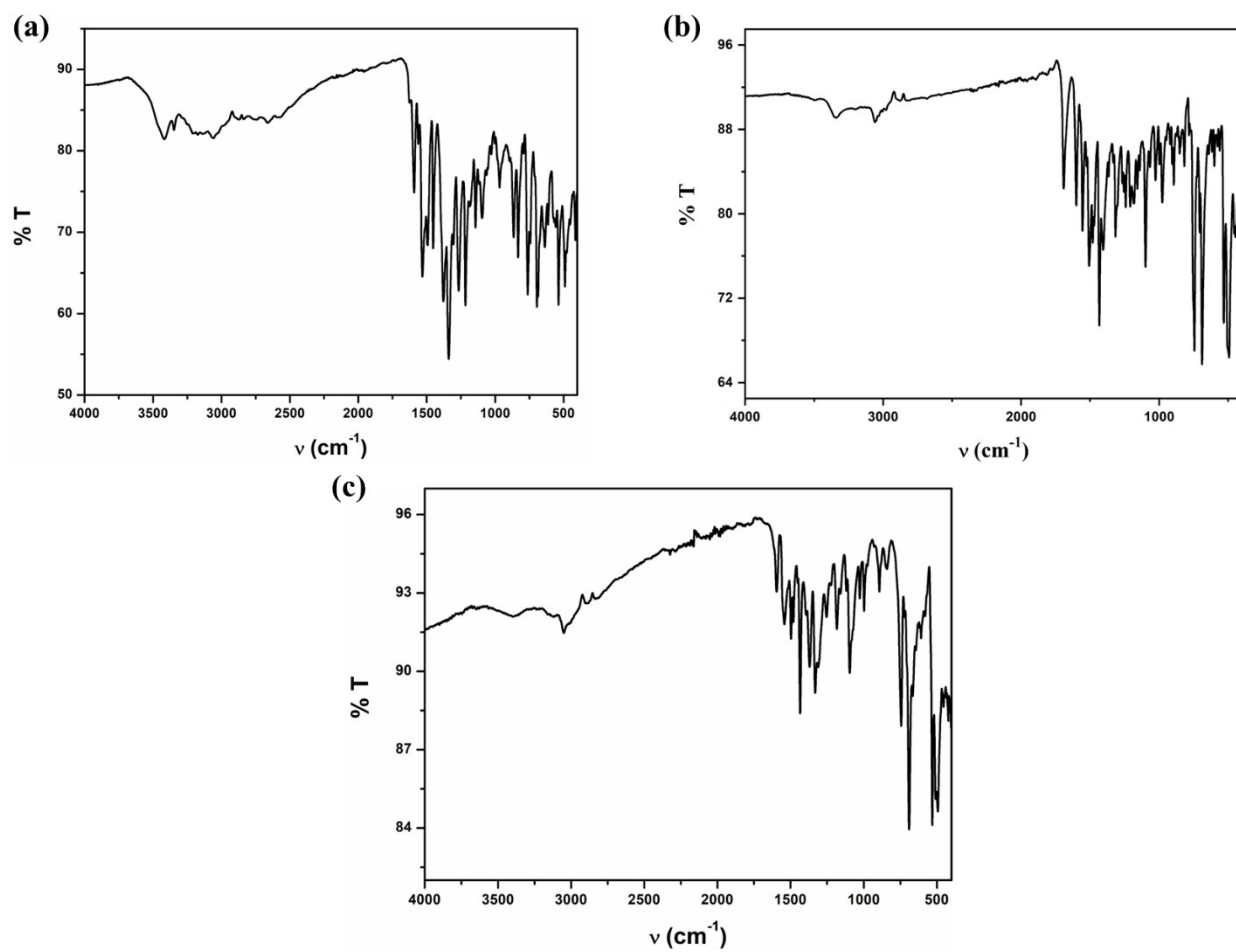
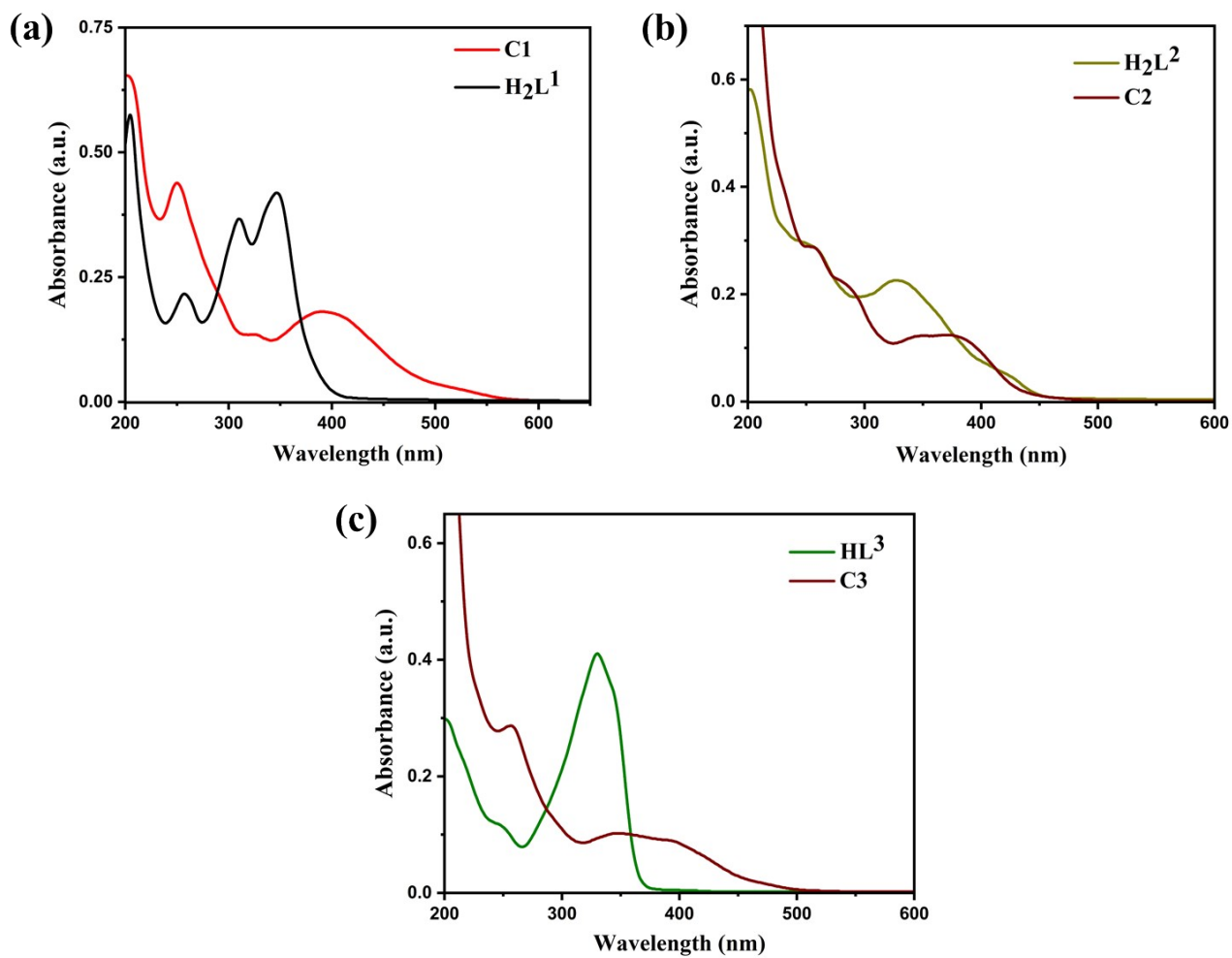
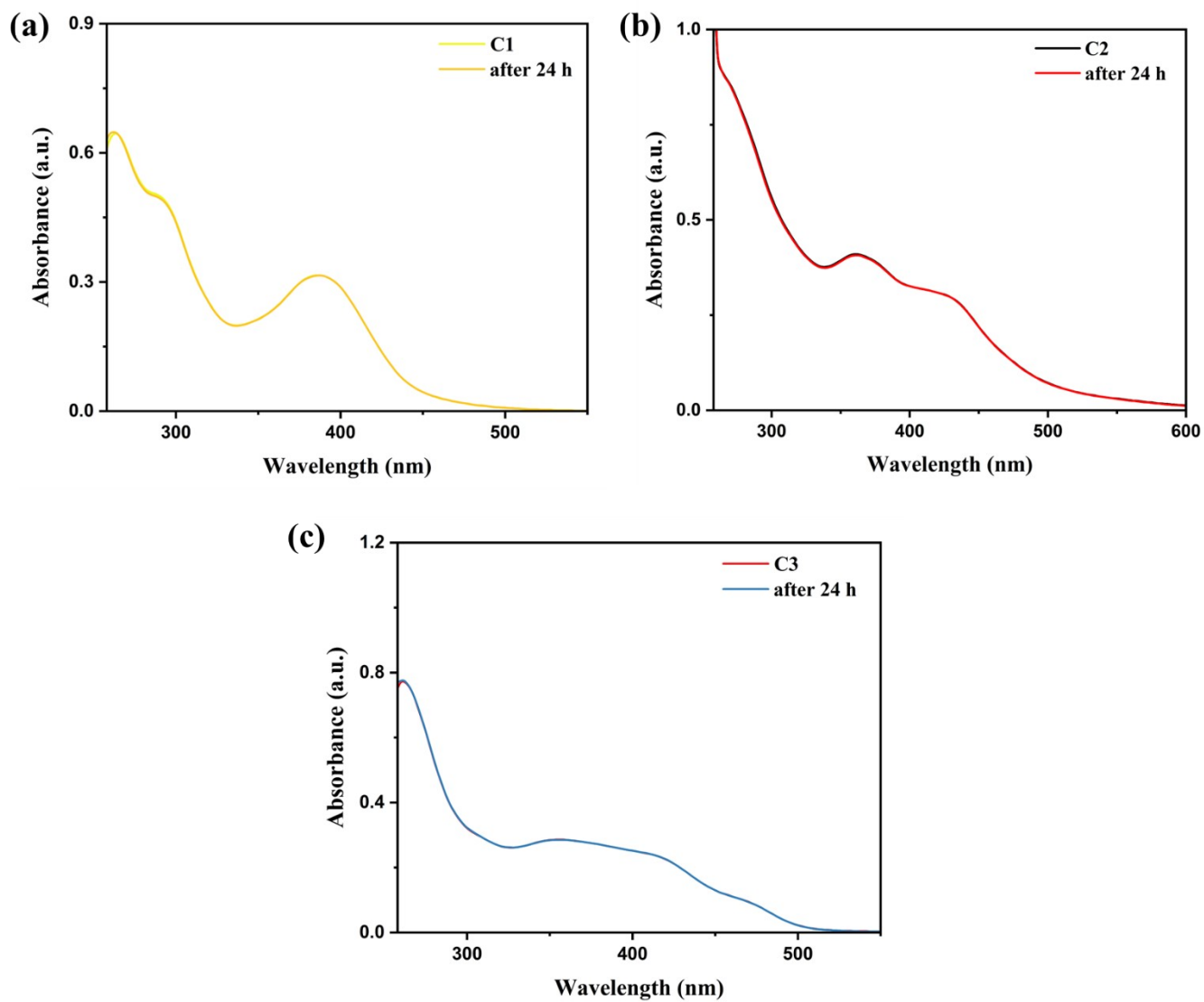


Figure S21: IR spectra of (a) C1, (b) C2 and (c) C3



**Figure S22:** UV-Vis spectra of (a)  $\text{H}_2\text{L}^1$  and **C1**, (b)  $\text{H}_2\text{L}^2$  and **C2** and (c)  $\text{HL}^3$  and **C3** in acetonitrile.  $[\text{H}_2\text{L}^1] = 1.5 \times 10^{-5}$  M,  $[\text{H}_2\text{L}^2] = 2 \times 10^{-5}$  M,  $[\text{HL}^3] = 1.3 \times 10^{-5}$  M,  $[\text{C1}] = 2 \times 10^{-5}$  M,  $[\text{C2}] = 1.2 \times 10^{-5}$  M and  $[\text{C3}] = 1 \times 10^{-5}$  M.



**Figure S23:** Time-dependent UV-Vis spectra of complexes (C1 – C3) in Tris-HCl/NaCl buffer (pH = 7.4) at room temperature.

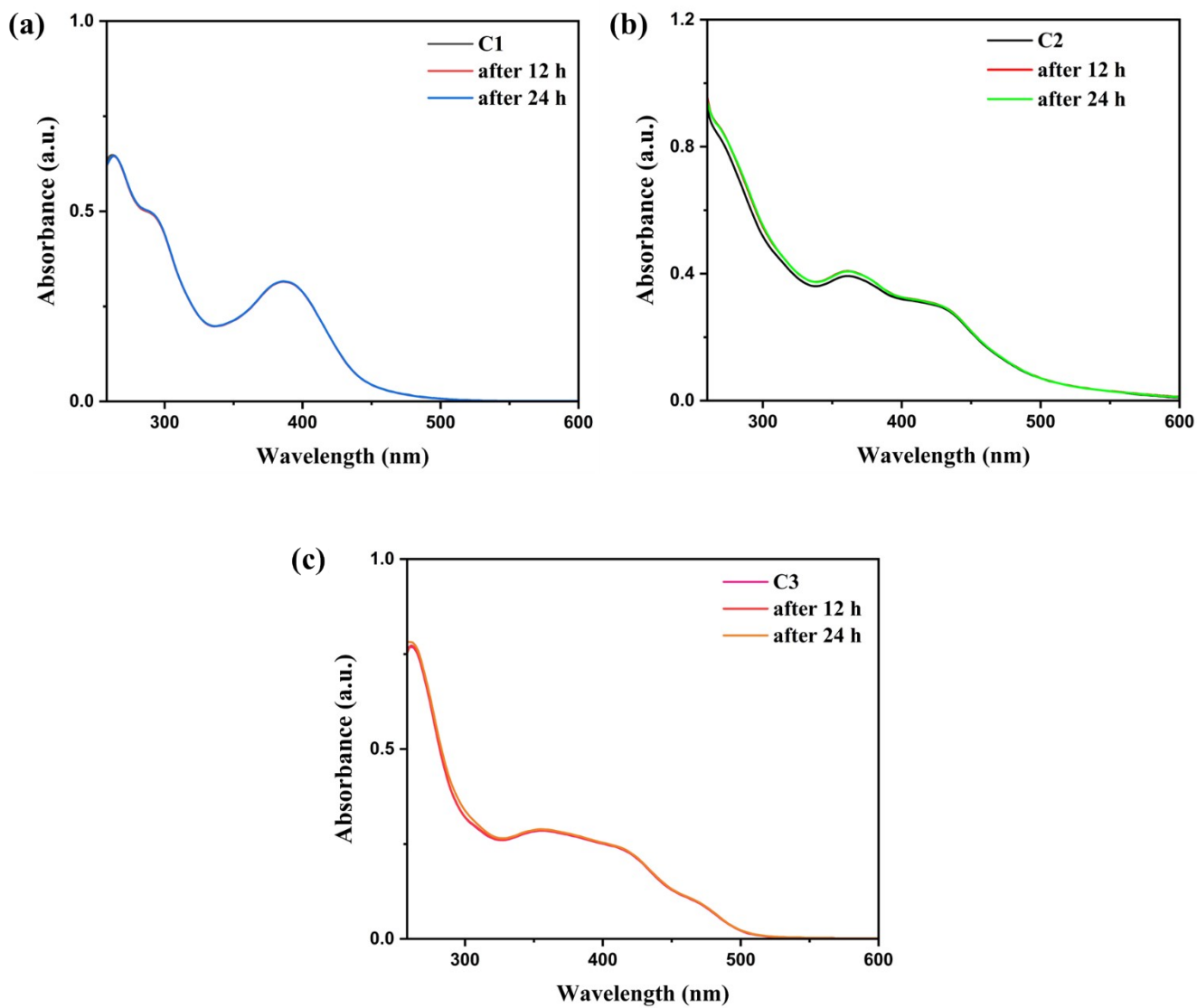


**Figure S24:** Time-dependent UV-Vis spectra of complexes (C1 – C3) in DMSO at room temperature.

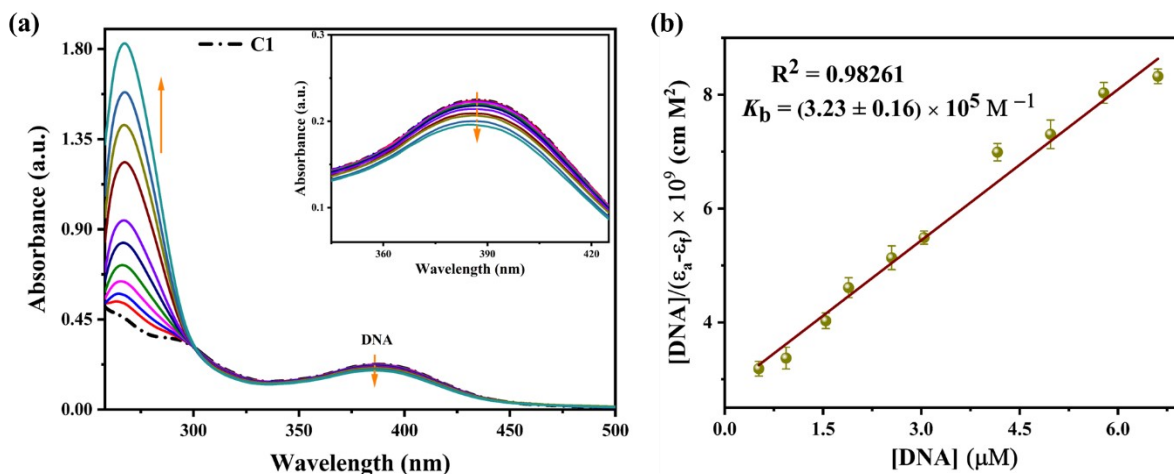


**Figure S25:** (a) UV-Vis titration of **C1** ( $2 \times 10^{-5}$  M) with the gradual addition of CT-DNA in Tris-HCl/NaCl buffer and (b) Wolfe-Shimmer plot of  $[DNA]/(\epsilon_a - \epsilon_f)$  vs  $[DNA]$ .

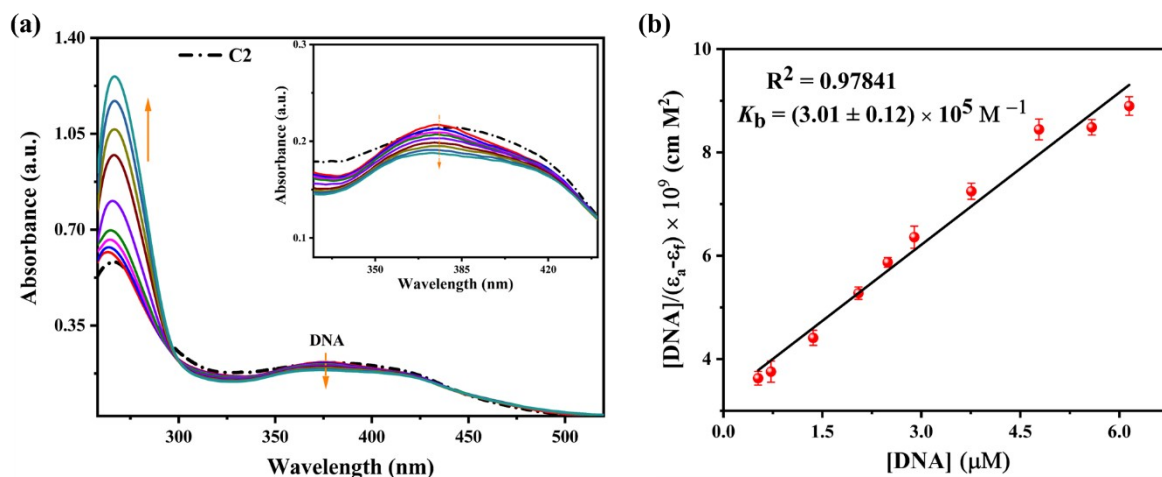


**Figure S26:** (a) UV-Vis titration of **C2** ( $2 \times 10^{-5}$  M) with the gradual addition of CT-DNA in Tris-HCl/NaCl buffer and (b) Wolfe-Shimmer plot of  $[DNA]/(\epsilon_a - \epsilon_f)$  vs  $[DNA]$ .

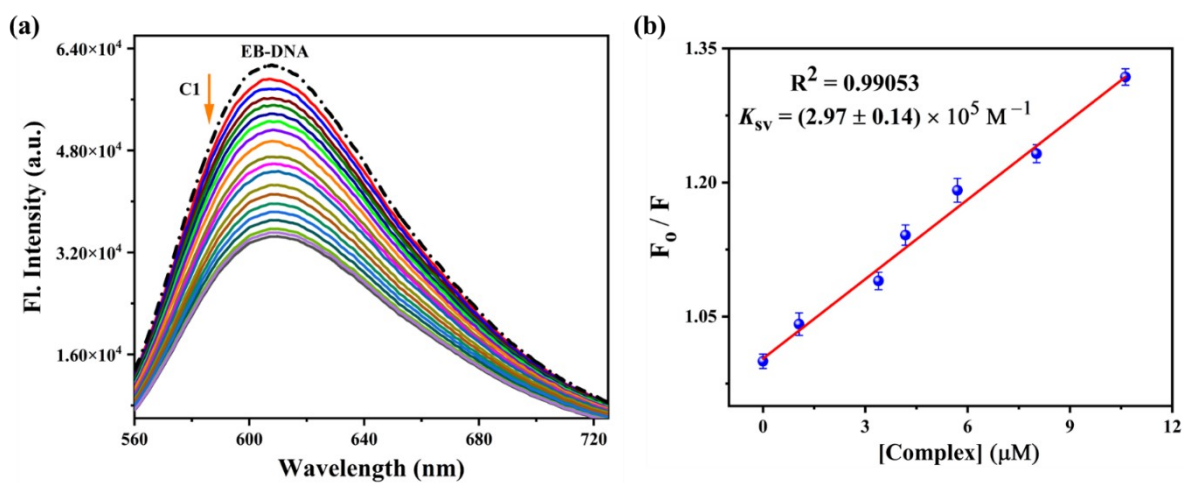


**Figure S27:** (a) Fluorescence titration of EB-CT DNA with the increasing amount of **C1** and (b) Stern-Volmer quenching plot of **C1**.

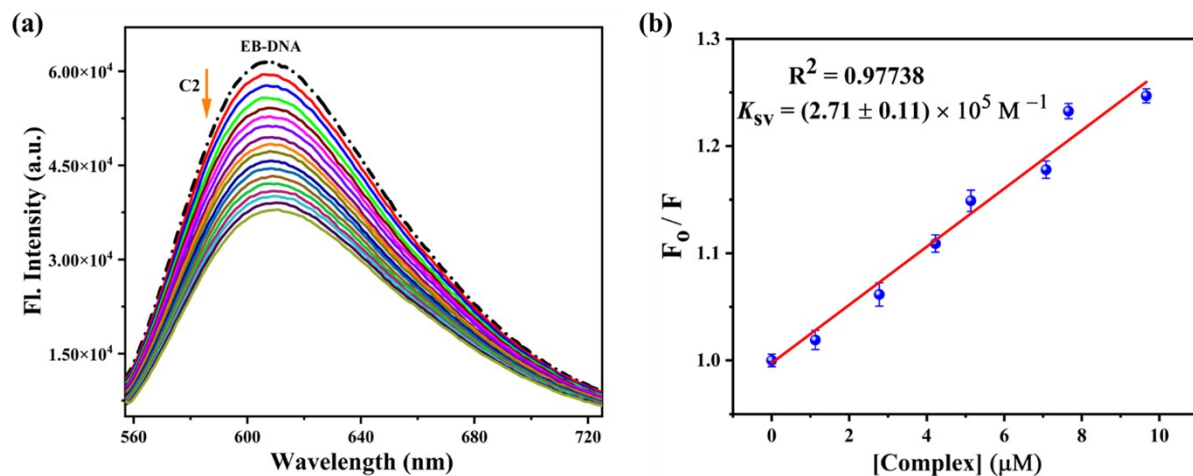


**Figure S28:** (a) Fluorescence titration of EB-CT DNA with the increasing amount of **C2** and (b) Stern-Volmer quenching plot of **C2**.

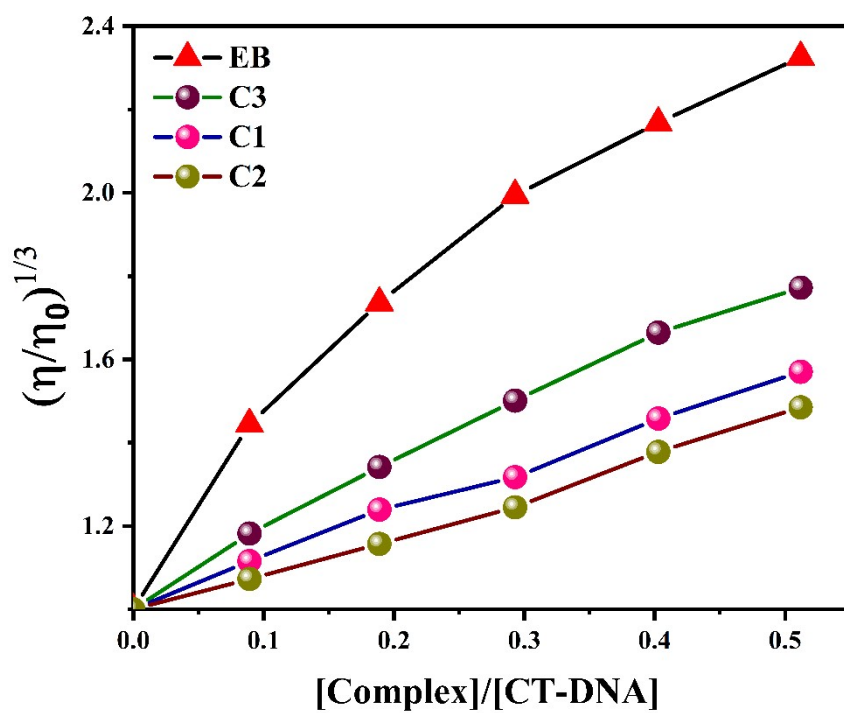


**Figure S29:** Effect of increasing concentrations of EB and complexes (**C1–C3**) on the relative viscosity of CT-DNA (30  $\mu\text{M}$ ) at 298 K.

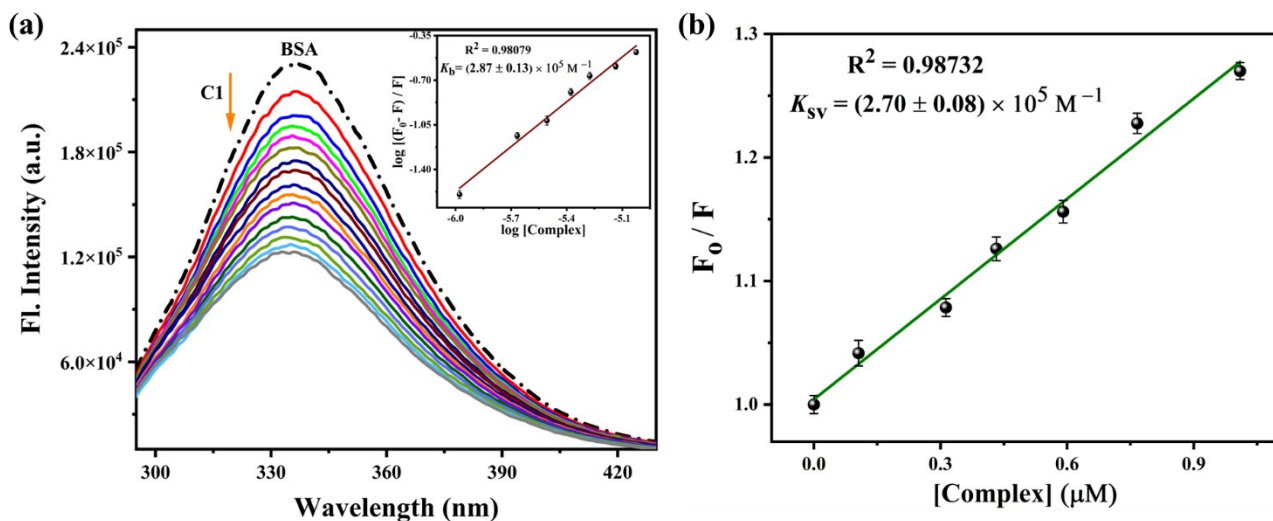


**Figure S30:** (a) Fluorescence quenching titration of BSA (5  $\mu\text{M}$ ) with incremental addition of **C1**. [Inset: Scatchard plot]. (b) Stern-Volmer plot of BSA for **C1**.

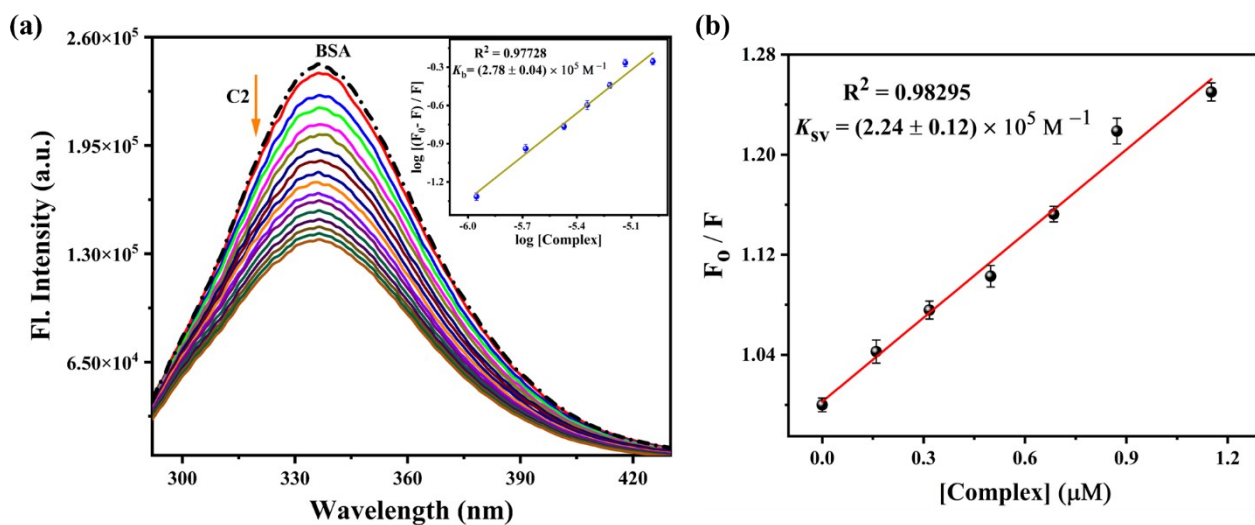


**Figure S31:** (a) Fluorescence quenching titration of BSA (5  $\mu\text{M}$ ) with incremental addition of **C2**. [Inset: Scatchard plot]. (b) Stern-Volmer plot of BSA for **C2**.

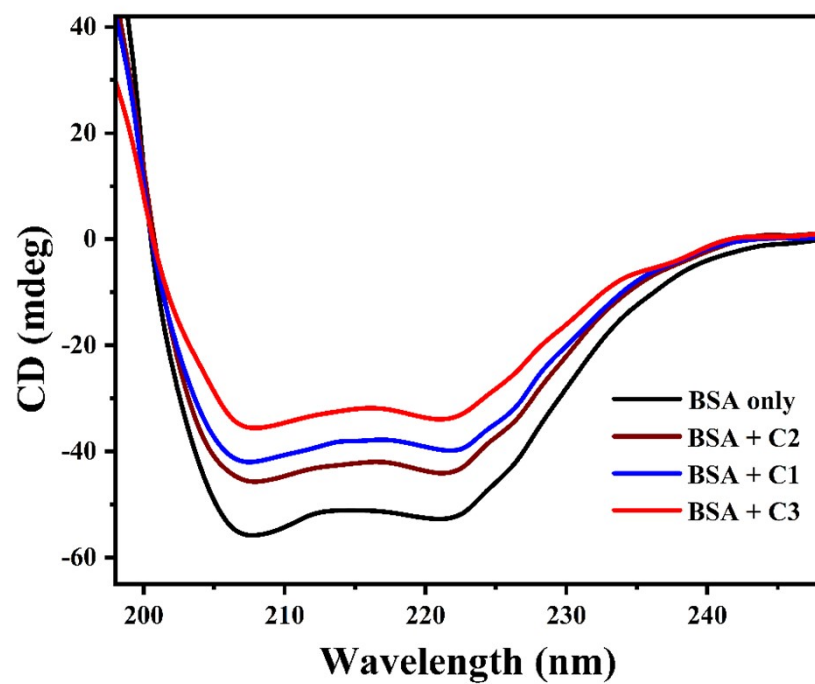


**Figure S32:** CD spectra of free BSA and BSA in presence of equimolar concentration of complexes C1–C3.

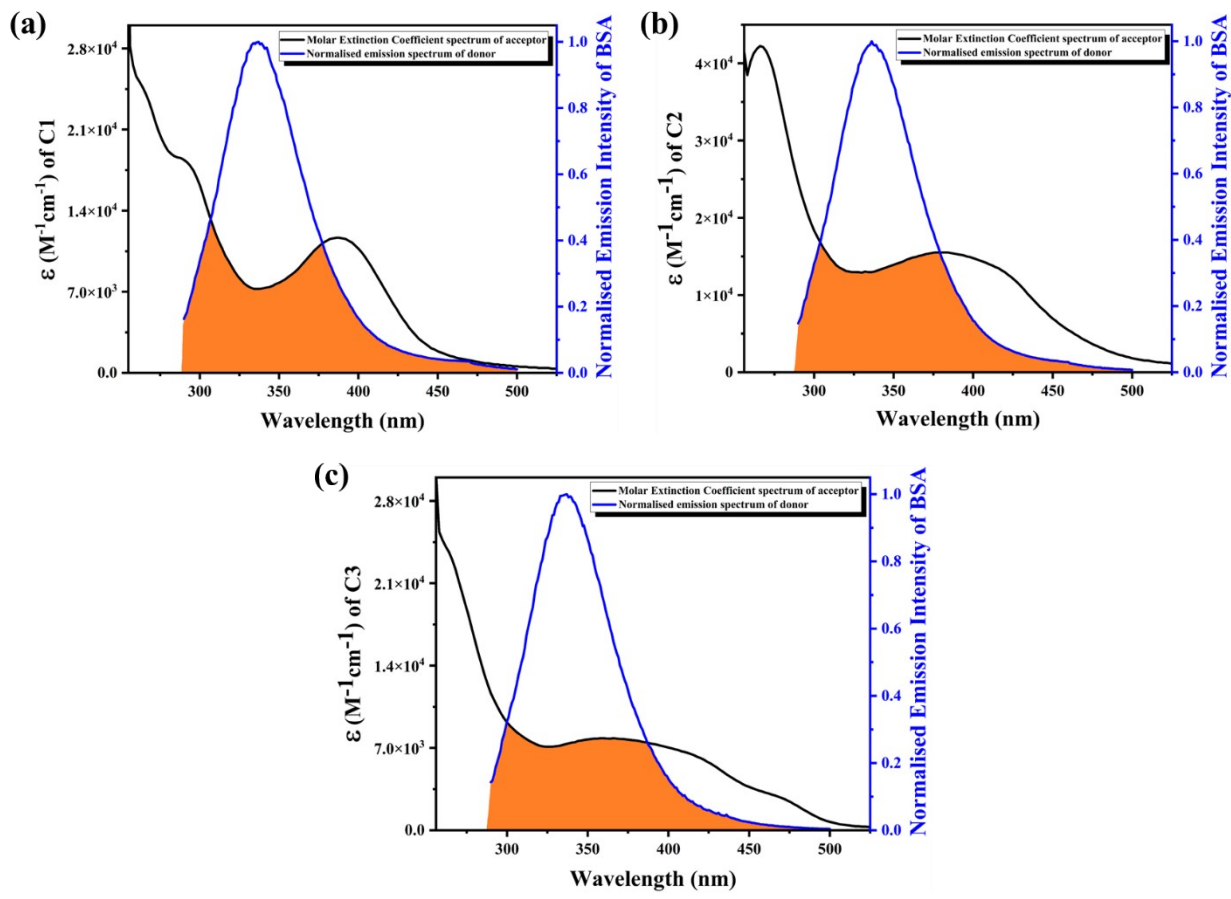
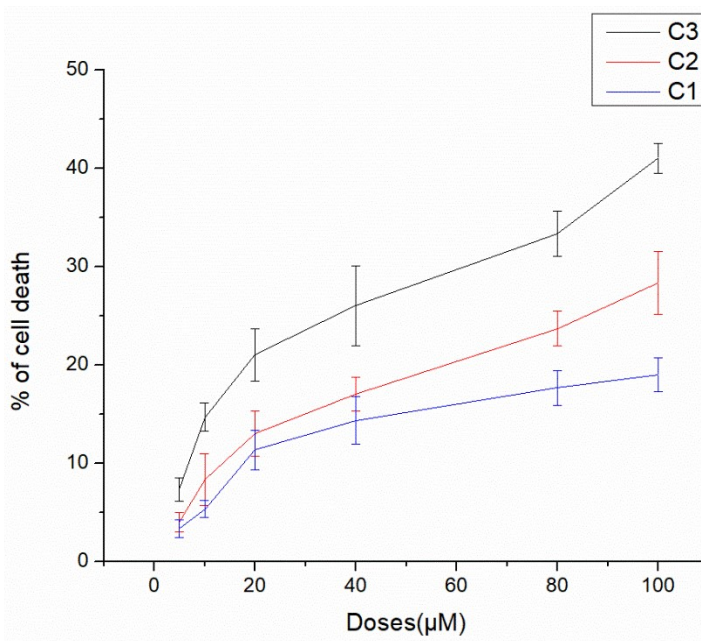


**Figure S33:** and complexes (c) **C3**. emission (blue), molar coefficient acceptor (black) shaded area spectral



FRET between BSA (a) **C1**, (b) **C2** and Normalised spectra of donor extinction spectrum of and the orange represent the overlap.

**Figure S34:** Assessment of cell viability using MTT assay. Viability of HepG2 cells were assessed by treating different doses of complexes **C1–C3**.

**Table S1:** Crystallographic data and refinement parameters of **HL<sup>3</sup>, C1, C2** and **C3**.

Compounds	<b>HL<sup>3</sup></b>	<b>C1</b>	<b>C2</b>	<b>C3</b>
Formula	C <sub>12</sub> H <sub>13</sub> N <sub>5</sub> S	C <sub>17</sub> H <sub>13</sub> ClN <sub>4</sub> OPdS	C <sub>36</sub> H <sub>28</sub> N <sub>3</sub> O <sub>3</sub> PPdS	C <sub>31</sub> H <sub>31</sub> ClN <sub>5</sub> OPPdS
Formula Weight	259.33	463.22	720.04	694.49
Crystal System	<i>orthorhombic</i>	<i>monoclinic</i>	<i>triclinic</i>	<i>monoclinic</i>
Space group	<i>P2<sub>1</sub>2<sub>1</sub>2<sub>1</sub></i>	<i>P2<sub>1</sub>/n</i>	<i>P -1</i>	<i>P2<sub>1</sub>/c</i>
a, b, c [Å]	5.8062(5), 14.1926(12), 15.6151(12)	7.7838(7), 15.0161(13), 14.8265(14)	10.1721(5), 12.4372(7), 13.8990(7)	8.3304(4), 18.3189(8), 20.2464(10)
α	90	90	75.234(2)	90
β	90	99.514(3)	72.327(2)	94.350(2)
γ	90	90	76.3060(10)	90
V [Å <sup>3</sup> ]	1286.76(18)	1709.1(3)	1595.66(15)	3080.8(3)
Z	4	4	2	4
D(calc) [g/cm <sup>3</sup> ]	1.339	1.800	1.499	1.497
Mu(MoKa) [ /mm]	0.241	1.377	0.738	0.842
F(000)	544	920	732	1416
Temperature (K)	293(2)	293(2)	293(2)	293(2)
Radiation [Å]	0.71073	0.71073	0.71073	0.71073
θ(Min-Max) [°]	2.978 - 25.053	1.944 - 25.036	2.133 – 26.999	2.692 - 27.511

Dataset (h; k; l)	-6 to 6, -16 to 16, -18 to 18	-9 to 9, -17 to 17, -12 to 17	-12 to 12, -15 to 15, -17 to 17	-10 to 10, -23 to 23, -26 to 26
R, $wR_2$	0.0610, 0.0983	0.0657, 0.0857	0.0253, 0.0592	0.0279, 0.0633
Goodness of fit(S)	1.046	1.086	0.941	1.065
CCDC No.	2287335	2287790	2287791	2287341

**Table S2:** Selected X-ray and calculated bond distances (Å) and angles (°) of **C1**, **C2** and **C3**

<b>C1</b>			<b>C2</b>			<b>C3</b>		
Bonds (Å)	X-ray	Calc.	Bonds (Å)	X-ray	Calc.	Bonds (Å)	X-ray	Calc.
Pd1–N2	1.949(5)	1.995	Pd1–O1	2.0082(15)	2.045	Pd1–N3	2.0336(16)	2.077
Pd1–N1	2.236(5)	2.238	Pd1–N1	2.0301(16)	2.054	Pd1–N1	2.1023(17)	2.138
Pd1–S1	2.234(2)	2.289	Pd1–S1	2.2274(6)	2.288	Pd1–S1	2.2484(5)	2.307
Pd1–Cl1	2.3221(19)	2.346	Pd1–P1	2.2755(5)	2.341	Pd1–P1	2.2690(5)	2.343
N2–N3	1.370(7)	1.352	N1–N2	1.399(2)	1.384	N1–C1	1.341(3)	1.347
N3–C11	1.317(8)	1.323	N2–C12	1.292(3)	1.298	N3–N4	1.373(2)	1.345
S1–C11	1.759(7)	1.774	S1–C12	1.755(2)	1.780	N4–C5	1.314(3)	1.323
O1–C1	1.367(8)	1.347				S1–C5	1.782(2)	1.790
<b>Angles (°)</b>								
N2–Pd1–N1	79.8(2)	79.702	O1–Pd1–N1	91.83(6)	91.164	N3–Pd1–N1	80.15(7)	79.282
N2–Pd1–S1	83.83(18)	83.358	O1–Pd1–S1	175.60(5)	174.901	N3–Pd1–S1	83.14(5)	82.025
N1–Pd1–S1	162.98(16)	162.947	N1–Pd1–S1	85.79(5)	84.544	N1–Pd1–S1	162.73(5)	161.167
N2–Pd1–Cl1	167.54(16)	170.184	O1–Pd1–P1	88.32(4)	88.3782	N3–Pd1–P1	175.13(5)	176.451
N1–Pd1–Cl1	108.46(16)	104.835	N1–Pd1–P1	177.57(5)	179.492	N1–Pd1–P1	104.40(5)	104.183
S1–Pd1–Cl1	88.45(7)	92.206	S1–Pd1–P1	94.220(19)	95.902	S1–Pd1–P1	92.442(19)	94.541
C11–S1–Pd1	95.9(2)	94.877						

**Table S3:** Selected X-ray and calculated bond distances and angles of **HL<sup>3</sup>**

Bonds (Å)	X-ray	Calc.
S1–C5	1.664(5)	1.677
N2–C1	1.321(6)	1.334
N3–C4	1.281(7)	1.292
N3–N4	1.370(6)	1.358
N4–C5	1.358(6)	1.384
C1–C4	1.442(7)	1.443

**Table S4:** Energy and % of composition of some selected molecular orbitals of [Pd(HL<sup>1</sup>)Cl] (**C1**)

MO	Energy	% of composition		
		Pd	HL <sup>1</sup>	Cl
LUMO+5	-0.14	02	98	00
LUMO+4	-0.33	00	100	00
LUMO+3	-0.65	01	99	00
LUMO+2	-1.59	03	97	00
LUMO+1	-2.46	44	45	11
LUMO	-3.02	05	95	00
HOMO	-5.89	13	83	04
HOMO-1	-6.07	05	94	01
HOMO-2	-6.38	05	88	07
HOMO-3	-6.71	52	24	23
HOMO-4	-6.82	34	20	46
HOMO-5	-6.97	50	16	34
HOMO-6	-7.13	00	100	00
HOMO-7	-7.42	05	82	13
HOMO-8	-7.66	13	66	21
HOMO-9	-8.02	26	72	04
HOMO-10	-8.16	27	49	24

**Table S5:** Energy and % of composition of some selected molecular orbitals of [Pd(L<sup>2</sup>)(PPh<sub>3</sub>)] (**C2**)

MO	Energy	% of composition		
		L <sup>2</sup>	Pd	PPh <sub>3</sub>
LUMO+5	-0.59	11	8	81
LUMO+4	-0.75	02	04	94
LUMO+3	-0.97	04	02	94
LUMO+2	-1.15	01	01	98
LUMO+1	-1.48	94	02	04
LUMO	-1.88	38	36	26
HOMO	-5.13	98	02	00
HOMO-1	-5.62	84	15	01
HOMO-2	-6.17	90	10	00
HOMO-3	-6.32	94	06	00
HOMO-4	-6.43	69	27	04
HOMO-5	-6.59	75	13	12
HOMO-6	-6.61	42	26	32
HOMO-7	-6.91	92	04	04
HOMO-8	-6.96	93	07	00
HOMO-9	-7.19	24	11	65
HOMO-10	-7.2	05	02	93

**Table S6:** Energy and composition of some selected molecular orbitals of [Pd(L<sup>3</sup>)(PPh<sub>3</sub>)]Cl (**C3**)

MO	Energy	% of composition		
		Pd	L <sup>3</sup>	PPh <sub>3</sub>
LUMO+5	-2.94	06	02	92
LUMO+4	-2.95	05	03	92
LUMO+3	-3.15	06	02	92
LUMO+2	-3.41	00	02	98
LUMO+1	-4.87	39	38	23
LUMO	-5.00	06	93	01
HOMO	-8.06	00	100	00
HOMO-1	-8.39	14	84	02
HOMO-2	-8.9	00	100	00
HOMO-3	-9.16	14	06	80
HOMO-4	-9.3	01	01	98
HOMO-5	-9.33	08	09	83
HOMO-6	-9.42	24	23	53
HOMO-7	-9.47	12	24	64
HOMO-8	-9.52	11	68	21
HOMO-9	-9.65	08	14	78
HOMO-10	-9.68	04	04	92

**Table S7:** Vertical electronic transition calculated by TDDFT/CPCM method of **C1**, **C2**, **C3** and **HL<sup>3</sup>**

Compd.	$\lambda$ (nm)	E (eV)	Osc. Strength (f)	Key excitations	Character	$\lambda_{\text{expt.}}$ (nm) ( $\epsilon$ , M <sup>-1</sup> cm <sup>-1</sup> )
<b>C1</b>	452.38	2.7407	0.2604	(21%) HOMO→LUMO+1	ILCT / LMCT	
	435.63	2.8461	0.2465	(80%) HOMO-2→LUMO	ILCT	391 (3045)
	306.43	4.0461	0.1908	(54%) HOMO-8→LUMO	ILCT / XLCT	325 (2274)
	305.09	4.0639	0.2060	(33%) HOMO-8→LUMO		
	251.08	4.9381	0.1504	(28%) HOMO-10→LUMO+1	ILCT/LMCT	250 (7370)
<b>C2</b>	396.40	3.1277	0.1494	(26%) HOMO-4→LUMO	ILCT/LMCT	
	385.56	3.2157	0.3897	(73%) HOMO→LUMO+1	ILCT	372 (4018)
	325.88	3.8046	0.1536	(53%) HOMO-5→LUMO	ILCT/LMCT	
	299.61	4.1382	0.0939	(21%) HOMO→LUMO+3	LXCT	
	287.79	4.3082	0.1737	(27%) HOMO→LUMO+4	LXCT	287

	255.16	4.8590	0.1070	(38%) HOMO→LUMO+9	ILCT	252
<b>C3</b>	448.55	2.7641	0.1353	(46%) HOMO→LUMO	ILCT	
	402.57	3.0798	0.5296	(43%) HOMO-1→LUMO	ILCT	348 (8121)
	336.76	3.6817	0.1227	(14%) HOMO-3→LUMO+1	XLCT/XMCT	
	281.29	4.4077	0.1239	(32%) HOMO-10→LUMO+1	XLCT/XMCT	257 (22837)
<b>HL<sup>3</sup></b>	348.61	3.5565	0.1812	(70%) HOMO-2→LUMO	n(L)→π*(L)	
	346.92	3.5738	0.8068	(75%) HOMO→LUMO	n(L)→π*(L)	330 (30770)
	320.17	3.8725	0.2173	(89%) HOMO-1→LUMO	n(L)→π*(L)	
	256.99	4.8244	0.1440	(61%) HOMO-1→LUMO+1	π(L)→π*(L)	
	250.18	4.9558	0.1826	(57%) HOMO→LUMO+2	π(L)→π*(L)	246 (8735)

[X = PPh<sub>3</sub>]

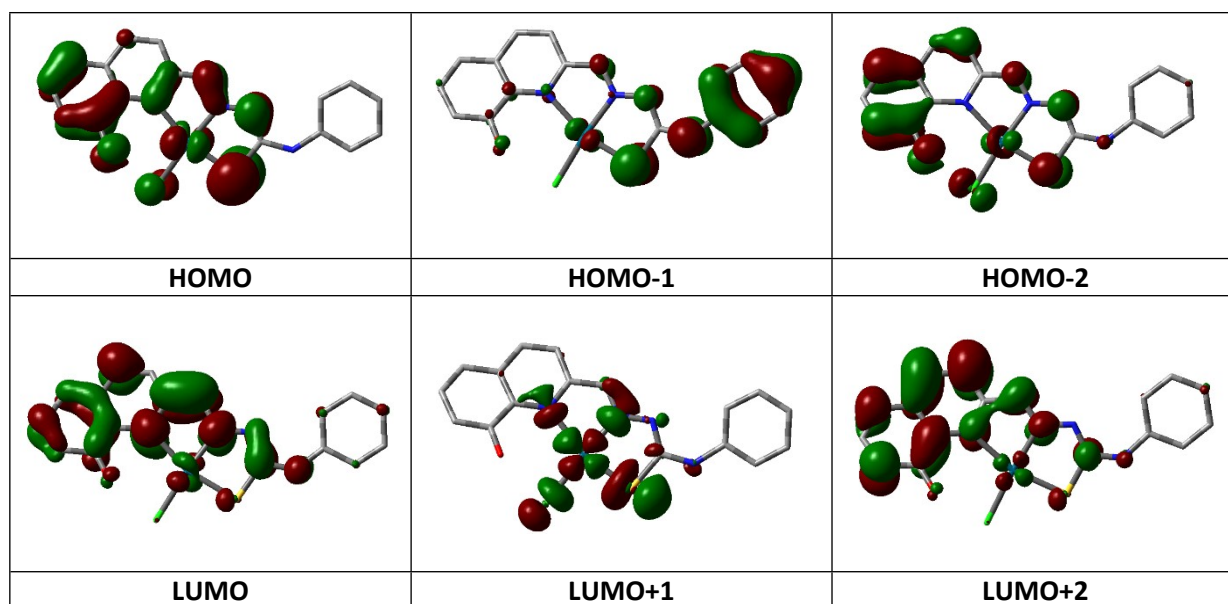


Figure S35: Contour plots of some selected molecular orbital of C1

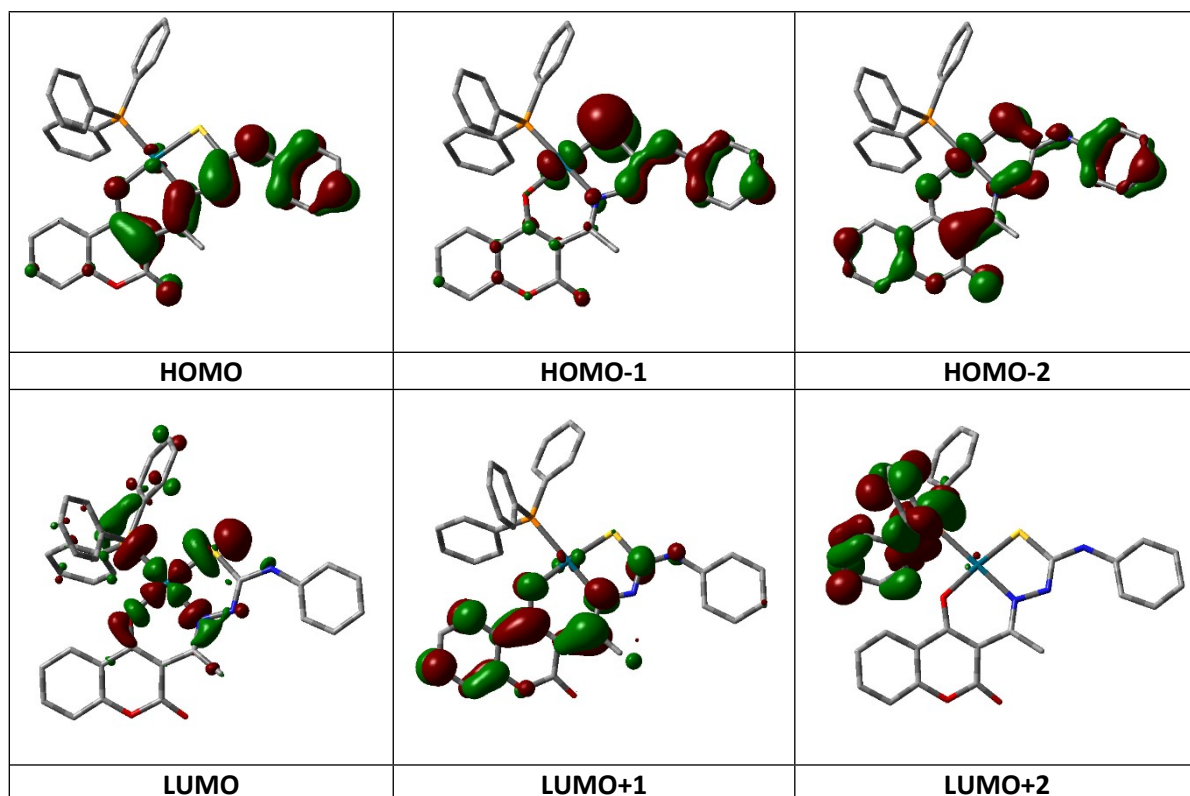


Figure S36: Contour plots of some selected molecular orbital of C2

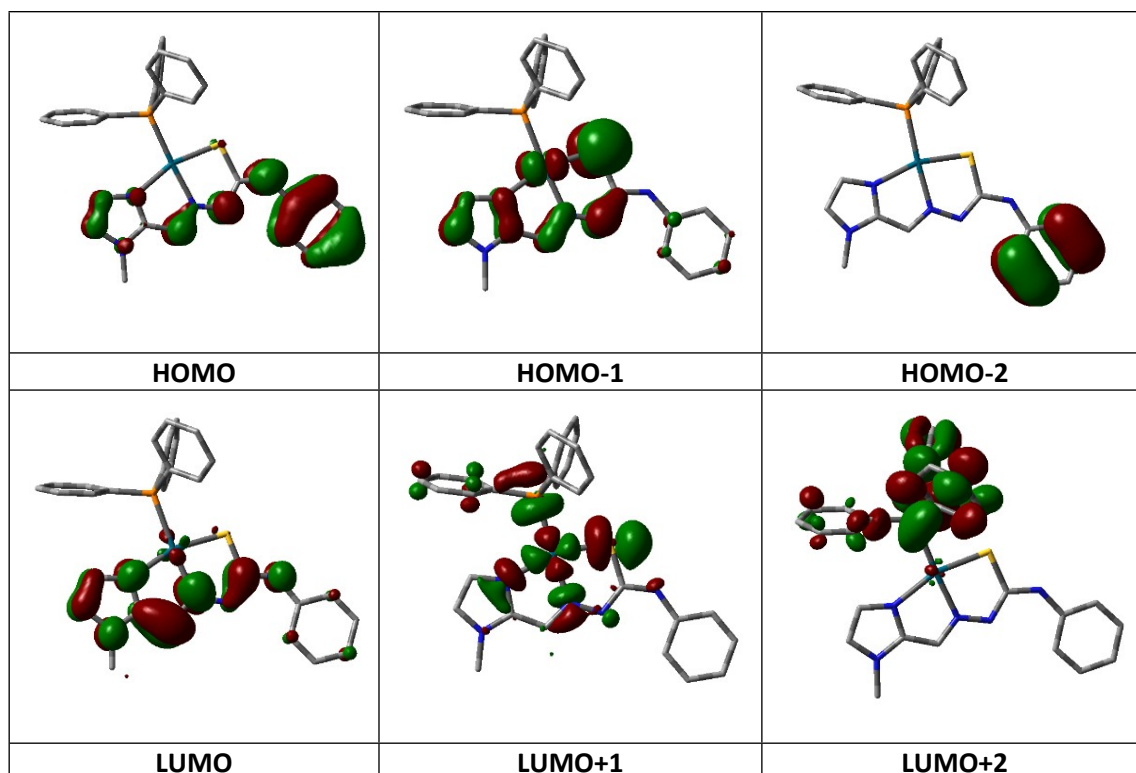


Figure S37: Contour plots of some selected molecular orbital of C3

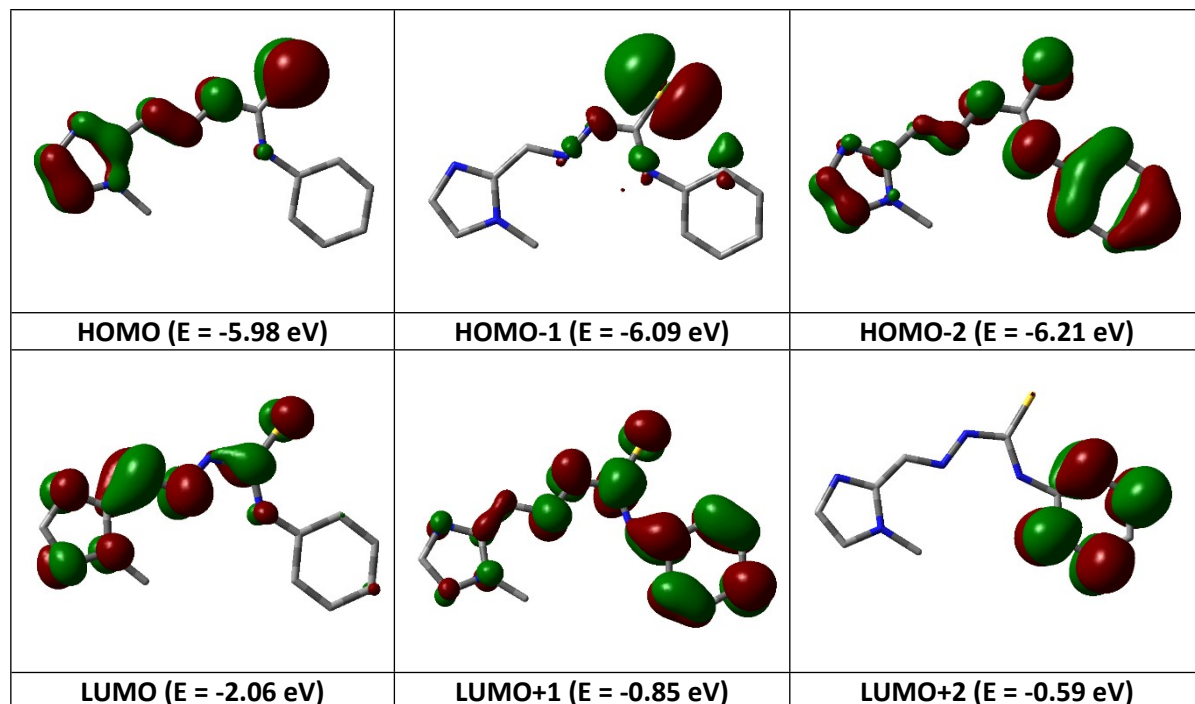


Figure S38: Contour plots of some selected molecular orbital of HL<sup>3</sup>

Table S8: Optimization of reaction conditions using catalyst **C1** for the model reaction

Entry	Solvent	Base	<b>C1</b> <sup>a</sup> (mol%)	Temp. (°C)	Time (h)	Yield <sup>b</sup> (%)	TON
1	EtOH	K <sub>2</sub> CO <sub>3</sub>	1	90	7	71	71
2	H <sub>2</sub> O	K <sub>2</sub> CO <sub>3</sub>	1	90	7	7	7
3	MeCN	K <sub>2</sub> CO <sub>3</sub>	1	90	7	22	22
4	i-PrOH	K <sub>2</sub> CO <sub>3</sub>	1	90	7	53	53
5	PEG-400	K <sub>2</sub> CO <sub>3</sub>	1	70	7	68	68
6	PEG-400	K <sub>2</sub> CO <sub>3</sub>	1	80	7	81	81
7	PEG-400	K <sub>2</sub> CO <sub>3</sub>	1	90	7	90	90
8	PEG-400	K <sub>2</sub> CO <sub>3</sub>	1	100	7	90	90
9	PEG-400	K <sub>2</sub> CO <sub>3</sub>	1	90	6	85	85
10	PEG-400	K <sub>2</sub> CO <sub>3</sub>	1	90	4	67	67
11	PEG-400	K <sub>2</sub> CO <sub>3</sub>	0.5	90	7	66	132
12	PEG-400	K <sub>2</sub> CO <sub>3</sub>	0.8	90	7	84	105
13	PEG-400	Na <sub>2</sub> CO <sub>3</sub>	1	90	7	88	88
14	PEG-400	NaOH	1	90	7	65	65

<sup>a</sup> Reaction conditions: **C1** (1 mol%), iodobenzene (1 mmol), phenylboronic acid (1 mmol), K<sub>2</sub>CO<sub>3</sub> (2 mmol), solvent 6 mL, 70-90°C, 7 h.

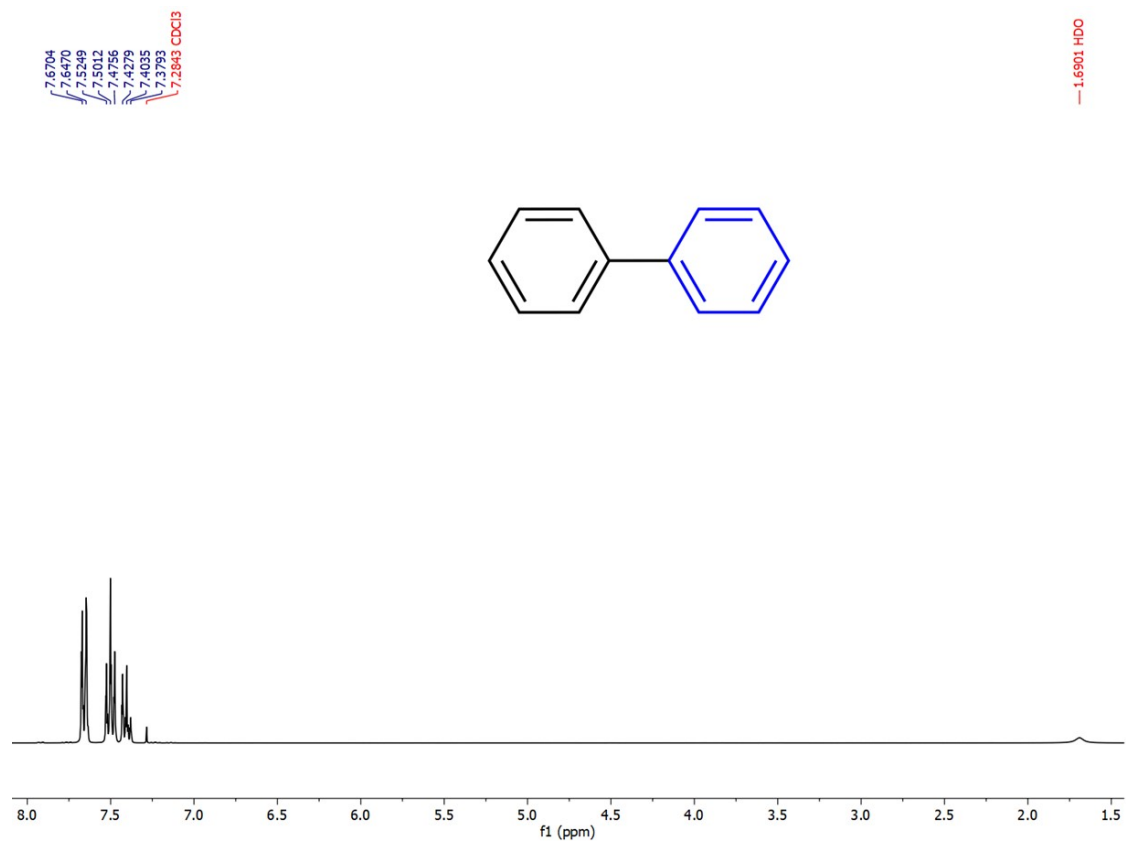
<sup>b</sup> Isolated yield after column chromatography.

Table S9: Optimization of reaction conditions using catalyst **C3** for the model reaction

Entry	Solvent	Base	<b>C3</b> <sup>a</sup> (mol%)	Temp. (°C)	Time (h)	Yield <sup>b</sup> (%)	TON
1	EtOH	K <sub>2</sub> CO <sub>3</sub>	1	90	6	76	76
2	H <sub>2</sub> O	K <sub>2</sub> CO <sub>3</sub>	1	90	6	18	18
3	MeCN	K <sub>2</sub> CO <sub>3</sub>	1	90	6	37	37
4	i-PrOH	K <sub>2</sub> CO <sub>3</sub>	1	90	6	65	65
5	PEG-400	K <sub>2</sub> CO <sub>3</sub>	1	70	6	75	75
6	PEG-400	K <sub>2</sub> CO <sub>3</sub>	1	80	6	87	87
7	PEG-400	K <sub>2</sub> CO <sub>3</sub>	1	90	6	95	95
8	PEG-400	K <sub>2</sub> CO <sub>3</sub>	1	100	6	95	95
9	PEG-400	K <sub>2</sub> CO <sub>3</sub>	1	90	5	90	90
10	PEG-400	K <sub>2</sub> CO <sub>3</sub>	1	90	4	77	77
11	PEG-400	K <sub>2</sub> CO <sub>3</sub>	0.5	90	6	74	148
12	PEG-400	K <sub>2</sub> CO <sub>3</sub>	0.8	90	6	89	111
13	PEG-400	Na <sub>2</sub> CO <sub>3</sub>	1	90	6	93	93
14	PEG-400	NaOH	1	90	6	66	66

<sup>a</sup> Reaction conditions: **C3** (1 mol%), iodobenzene (1 mmol), phenylboronic acid (1 mmol), K<sub>2</sub>CO<sub>3</sub> (2 mmol), solvent 6 mL, 70-90°C, 6 h.

<sup>b</sup> Isolated yield after column chromatography .



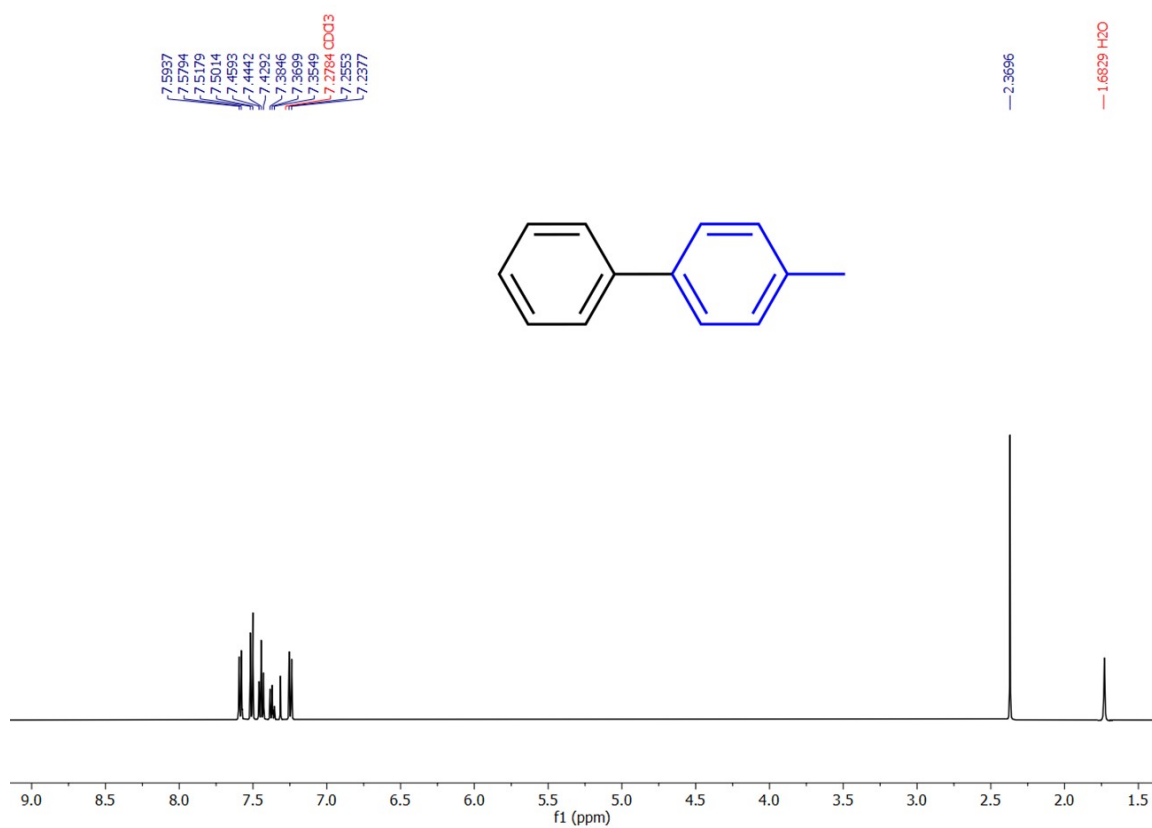


Figure S40:  $^1\text{H}$  NMR of 4-methyl-1,1'-biphenyl

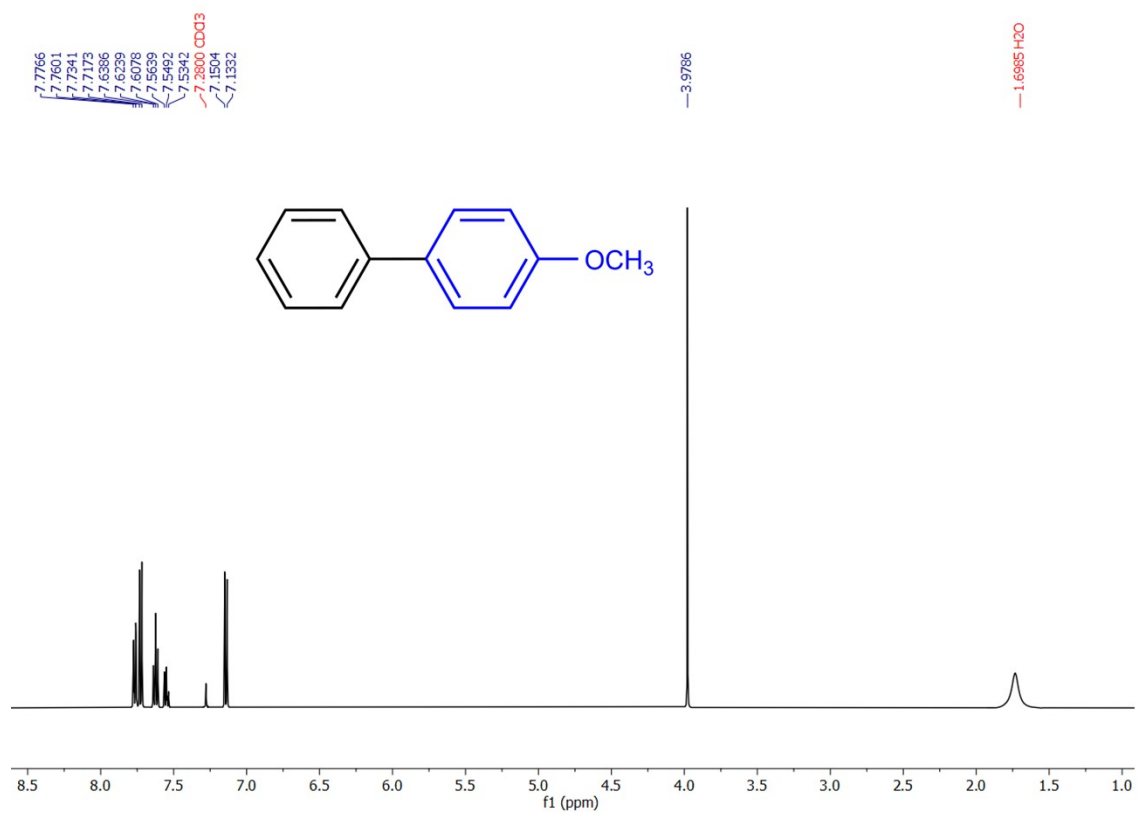


Figure S41:  $^1\text{H}$  NMR of 4-methoxy-1,1'-biphenyl

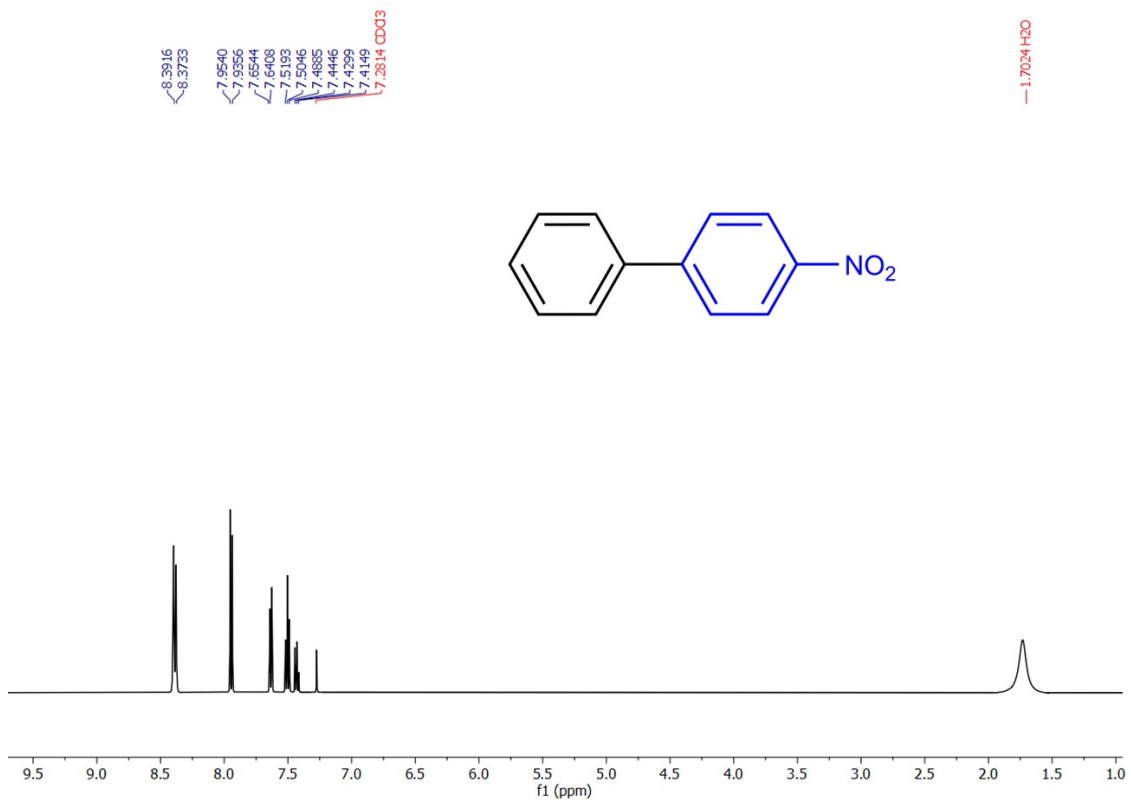


Figure S42: <sup>1</sup>H NMR of 4-nitro-1,1'-biphenyl

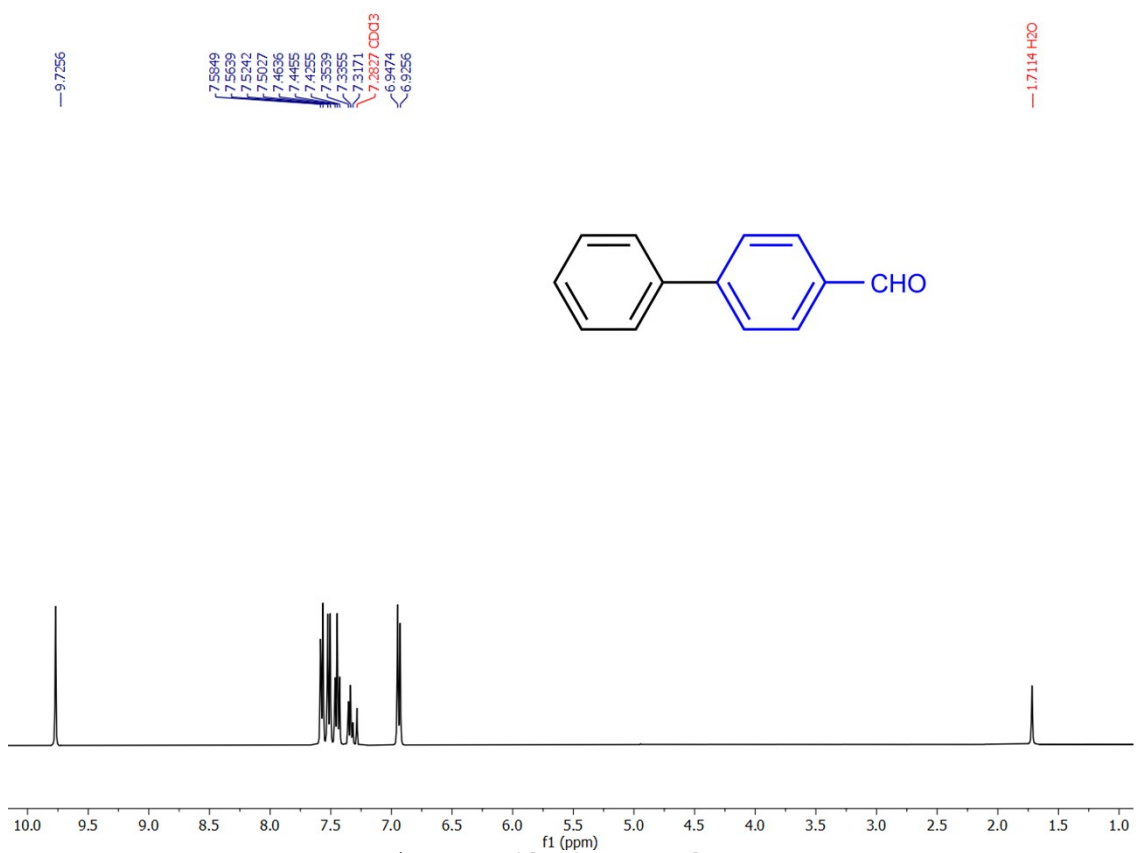
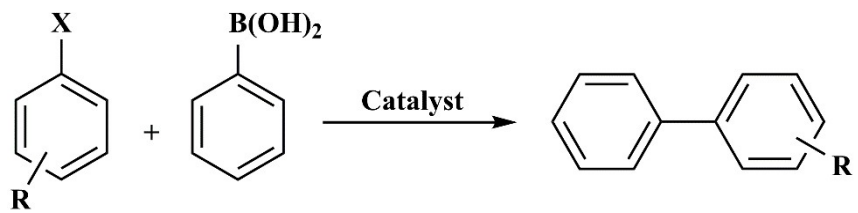
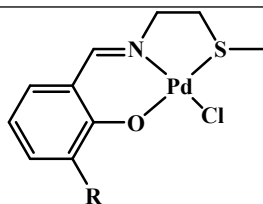
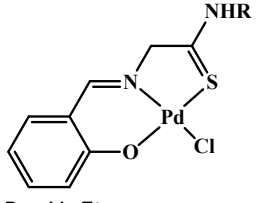
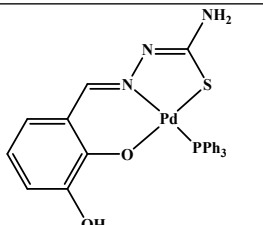
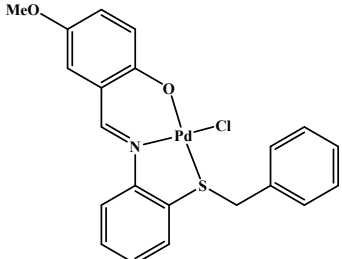
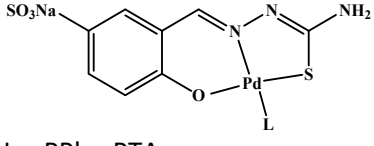
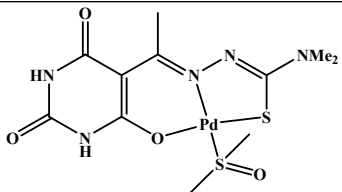
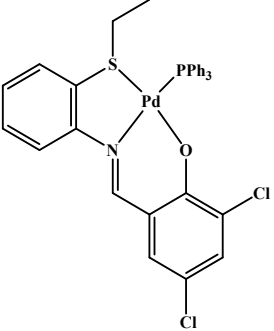
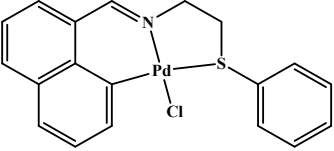
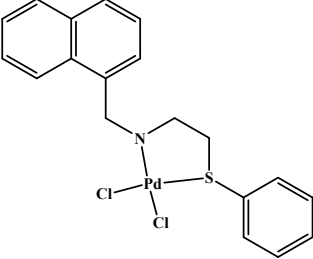
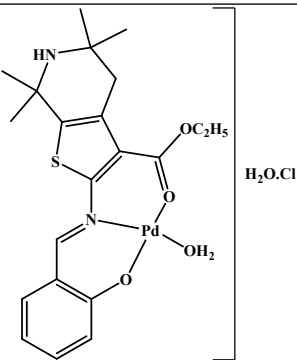
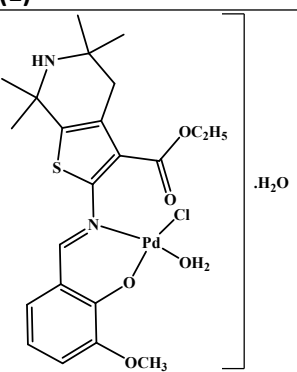
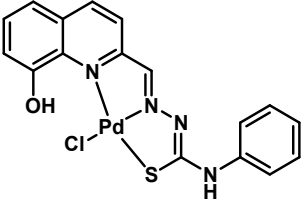
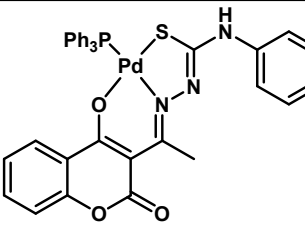
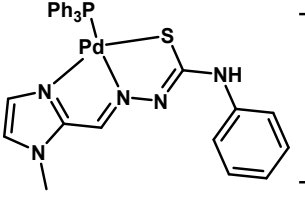


Figure S43: <sup>1</sup>H NMR of [1,1'-biphenyl]-4-carbaldehyde

**Table S10:** Comparison of catalytic efficiency and reaction conditions of Suzuki-Miyaura cross-coupling reactions by palladium complexes with O N S donor ligands.

									
Catalysts	R	X	Mol% (cat.)	Solvent	Temp. (°C)	Time (h)	Yield (%)	Ton	Ref.
 R = H, CH(CH <sub>2</sub> CH <sub>3</sub> ) <sub>2</sub>	H OCH <sub>3</sub> NO <sub>2</sub>	Br Br Br	0.2	DMF/ H <sub>2</sub> O	100	24	45 25 100	225 125 500	12
 R = H, Et	H OCH <sub>3</sub> NO <sub>2</sub> H	Br Br Br Cl	0.1	DMF/ H <sub>2</sub> O	100	24	71 53 83 30	710 530 830 300	13
	H	Br	0.08	i-PrOH	80	6	92	1150	14
	H H	I Br	1	MeOH	65	24	92 90	92 90	15
 L = PPh <sub>3</sub> , PTA	H CH <sub>3</sub> OCH <sub>3</sub>	Br Br Br	1	H <sub>2</sub> O	70	24	76 72 93	76 72 93	16
	H H OCH <sub>3</sub> NO <sub>2</sub>	Br Cl Br Br	2	DMF	140	24	46 21 66 78	23 11 33 39	17

	H H H CH <sub>3</sub> OCH <sub>3</sub> NO <sub>2</sub>	Cl Br I Br Br Br	1	PEG-400	100	10	83 93 96 90 93 88	83 93 96 90 93 88	18
 <p>(Complex 1)</p>	H OCH <sub>3</sub> NO <sub>2</sub> CH <sub>3</sub>	Br Br Br Br	0.05/0. 1 0.1 0.01 0.05/0. 1	DMF/ H <sub>2</sub> O	90	6/2 6 2 6/2	80/96 88 96 71/97	1600/960 880 9600 1420/970	19
 <p>(Complex 3)</p>	H OCH <sub>3</sub> NO <sub>2</sub> CH <sub>3</sub>	Br Br Br Br	0.05/0. 1 0.1 0.01 0.05/0. 1	DMF/ H <sub>2</sub> O	90	6/2 6 2 6/2	21/74 68 94 69/88	420/740 680 9400 1380/880	
 <p>(1)</p>	H CH <sub>3</sub> OCH <sub>3</sub> CHO	Br Br Br Br	0.01	EtOH/H <sub>2</sub> O	80	2	98 67 91 91	9800 6700 9100 9100	20
 <p>(2)</p>	H CH <sub>3</sub> OCH <sub>3</sub> CHO	Br Br Br Br	0.01	EtOH/H <sub>2</sub> O	80	2	99 71 70 95	9900 7100 7000 9500	

 <p>(C1)</p>	H H H CH <sub>3</sub> CH <sub>3</sub> OCH <sub>3</sub> OCH <sub>3</sub> NO <sub>2</sub> CHO	I Br Cl I Br I Br Br Br	1	PEG-400	90	7	90 85 78 86 81 85 82 73 75	90 85 78 86 81 85 82 73 75	<b>This Work</b>	
 <p>(C2)</p>	H H H CH <sub>3</sub> CH <sub>3</sub> OCH <sub>3</sub> OCH <sub>3</sub> NO <sub>2</sub> CHO	I Br Cl I Br I Br Br Br	1	PEG-400	90	6	97 94 88 95 94 94 93 87 88	97 94 88 95 94 94 93 87 88		
 <p>(C3)</p>	H H H CH <sub>3</sub> CH <sub>3</sub> OCH <sub>3</sub> OCH <sub>3</sub> NO <sub>2</sub> CHO	I Br Cl I Br I Br Br Br	1	PEG-400	90	6	95 91 85 92 90 91 89 83 85	95 91 85 92 90 91 89 83 85		

## References

1. Bruker. SAINT v8.38A. Bruker AXS Inc., Madison, Wisconsin, USA.
2. L. Krause, R. Herbst-Irmer, G. M. Sheldrick, D. Stalke, *J. Appl. Cryst.*, 2015, **48**, 3-10.
3. (a) G. M. Sheldrick, *Acta Cryst.*, 2008, **A64**, 112-122. (b) G. M. Sheldrick, *Acta Cryst.*, 2015, **C71**, 3-8.
4. (a) A. D. Becke, *J. Chem. Phys.*, 1993, **98**, 5648-5652; (b) C. Lee, W. Yang, R. G. Parr, *Phys. Rev. B: Condens. Matter Mater. Phys.*, 1988, **37**, 785-789.
5. (a) P. J. Hay and W. R. Wadt, *J. Chem. Phys.*, 1985, **82**, 270; (b) W. R. Wadt and P. J. Hay, *J. Chem. Phys.*, 1985, **82**, 284; (c) P. J. Hay and W. R. Wadt, *J. Chem. Phys.*, 1985, **82**, 299.
6. M. J. Frisch, G. W. Trucks, H. B. Schlegel, G. E. Scuseria, M. A. Robb, J. R. Cheeseman, G. Scalmani, V. Barone, B. Mennucci, G. A. Petersson, H. Nakatsuji, M. Caricato, X. Li, H. P. Hratchian, A. F. Izmaylov, J. Bloino, G. Zheng, J. L. Sonnenberg, M. Hada, M. Ehara, K. Toyota, R. Fukuda, J. Hasegawa, M. Ishida, T. Nakajima, Y. Honda, O. Kitao, H. Nakai, T. Vreven, J. A. Montgomery, Jr., J. E. Peralta, F. Ogliaro, M. Bearpark, J. J. Heyd, E. Brothers, K. N. Kudin, V. N.

- Staroverov, R. Kobayashi, J. Normand, K. Raghavachari, A. Rendell, J. C. Burant, S. S. Iyengar, J. Tomasi, M. Cossi, N. Rega, J. M. Millam, M. Klene, J. E. Knox, J. B. Cross, V. Bakken, C. Adamo, J. Jaramillo, R. Gomperts, R. E. Stratmann, O. Yazyev, A. J. Austin, R. Cammi, C. Pomelli, J. W. Ochterski, R. L. Martin, K. Morokuma, V. G. Zakrzewski, G. A. Voth, P. Salvador, J. J. Dannenberg, S. Dapprich, A. D. Daniels, O. Farkas, J. B. Foresman, J. V. Ortiz, J. Cioslowski and D. J. Fox, Gaussian 09, Revision D.01, Gaussian, Inc., Wallingford CT, **2009**.
7. (a) R. Bauernschmitt and R. Ahlrichs, *Chem. Phys. Lett.*, 1996, **256**, 454; (b) R. E. Stratmann, G. E. Scuseria and M. J. Frisch, *J. Chem. Phys.*, 1998, **109**, 8218; (c) M. E. Casida, C. Jamorski, K. C. Casida and D. R. Salahub, *J. Chem. Phys.*, 1998, **108**, 4439.
  8. (a) V. Barone and M. Cossi, *J. Phys. Chem. A*, 1998, **102**, 1995; (b) M. Cossi and V. Barone, *J. Chem. Phys.*, 2001, **115**, 4708; (c) M. Cossi, N. Rega, G. Scalmani and V. Barone, *J. Comput. Chem.*, 2003, **24**, 669.
  9. N. M. O'Boyle, A. L. Tenderholt and K. M. Langner, *J. Comput. Chem.*, 2008, **29**, 839.
  10. A. Banerjee, M. Mohanty, S. Lima, R. Samanta, E. Garribba, T. Sasamori and R. Dinda, *New J. Chem.*, 2020, **44**, 10946–10963.
  11. S. U. Parsekar, P. Velankanni, S. Sridhar, P. Haldar, N. A. Mate, A. Banerjee, P. K. S. Antharjanam, A. P. Koley and M. Kumar, *Dalton Trans.*, 2020, **49**, 2947–2965.
  12. I. D. Kostas, B. R. Steele, A. Terzis, S. V. Amosova, A. V. Martynov and N. A. Makhaeva, *Eur. J. Inorg. Chem.*, 2006, **2006**, 2642–2646.
  13. I. D. Kostas, F. J. Andreadaki, D. Kovala-Demertzi, P. Christos and M. A. Demertzis, *Tetrahedron Lett.*, 2005, **46**, 1967–1970.
  14. B. Agrahari, S. Layek, Anuradha, R. Ganguly and D. D. Pathak, *Inorg. Chim. Acta*, 2018, **471**, 345–354.
  15. M. Kalita, K. J. Tamuli, P. Barman, B. Sarma, R. Baruah and H. P. D. Boruah, *Polyhedron*, 2015, **97**, 140–147.
  16. L. C. Matsinha, J. Mao, S. F. Mapolie and G. S. Smith, *Eur. J. Inorg. Chem.*, 2015, **2015**, 4088–4094.
  17. A. Castiñeiras, N. Fernández-Hermida, I. García-Santos and L. Gómez-Rodríguez, *Dalton Trans.*, 2012, **41**, 13486-13495.
  18. C. K. Manna, R. Naskar, B. Bera, A. Das and T. K. Mondal, *J. Mol. Struct.*, 2021, **1237**, 130322.
  19. R. Bhaskar, A. K. Sharma, M. K. Yadav and A. K. Singh, *Dalton Trans.*, 2017, **46**, 15235-15248.
  20. A. Akdeniz and N. Turan, *J. Mol. Struct.*, 2023, **1287**, 135724.